Journal of Structural Geology 37 (2012) 1–18

Contents lists available at SciVerse ScienceDirect

Journal of Structural Geology

journal homepage: www.elsevier.com/locate/jsg

Polystage deformation of the Gaoligong metamorphic zone: Structures, $^{40}Ar/^{39}Ar$ mica ages, and tectonic implications

Bo Zhang [a,*], Jinjiang Zhang [a], Dalai Zhong [b], Liekun Yang [b], Yahui Yue [c], Shuyu Yan [a]

[a] The Key Laboratory of Orogenic Belts and Crustal Evolution, School of Earth and Space Sciences, Peking University, Beijing 100871, China
[b] Institute of Geology and Geophysics, Chinese Academy of Sciences, Beijing 100029, China
[c] Key Laboratory of Continental Collision and Plateau Uplift, Institute of Tibetan Plateau Research, Chinese Academy of Sciences, Beijing 100085, China

ARTICLE INFO

Article history:
Received 26 August 2011
Received in revised form
1 February 2012
Accepted 5 February 2012
Available online 14 February 2012

Keywords:
Structure
CPOs
Polystage deformation
$^{40}Ar/^{39}Ar$
Gaoligong metamorphic zone

ABSTRACT

The Gaoligong metamorphic zone is located southeast of the Eastern Himalayan Syntaxis in western Yunnan, China. The zone is characterized by four stages of deformation (D1–D4). D1 structures record early compressive deformation during the Indosinian orogeny, which formed tight to isoclinal F1 folds of bedding with a penetrative S1 foliation developed parallel to fold axial planes. Mid-crustal horizontal shearing during D2 resulted in overprinting of D1 structures. D1 and D2 structures are associated with granulite facies metamorphism. D3 doming resulted in late crustal thickening and the development of a regional NW–SE trending F3 antiform. Synchronous with or slightly subsequent to D3 deformation, the zone experienced D4 ductile strike-slip shearing, resulting in its exhumation to shallow crustal levels and retrograde metamorphism. Granitic D4 mylonites predominantly yield $^{40}Ar/^{39}Ar$ mica ages of 15–16 Ma, indicating that D4 dextral strike-slip shearing occurred in the Miocene. Weakly deformed leucogranite and protomylonite yield $^{40}Ar/^{39}Ar$ ages of 10–11 Ma, suggesting that ductile strike-slip shearing continued to the Late Miocene. The new $^{40}Ar/^{39}Ar$ data indicate that escape-related deformation along the Gaoligong strike-slip shear zone occurred in the Miocene. In association with recent geophysical studies, and on the basis of the structural, crystal preferred orientation (CPO), and geochronological data presented in this paper, we suggest that the Gaoligong metamorphic zone formed in response to intracontinental transpression in the southeast of Tibet, characterized as intense deformation and metamorphism at middle–upper crustal levels.

1. Introduction

The intracontinental deformation that characterizes much of southeastern Asia has been well studied, providing insight into the Tertiary collision between India and Eurasia (e.g., Tapponnier et al., 1982; Leloup et al., 1995; Wang and Burchfiel, 1997; Yin and Harrison, 2000; Zhong, 2000; Searle, 2006; Morley, 2007). Tapponnier et al. (1982, 2001) used the indentation–extrusion tectonic model to elucidate the nature of India–Eurasia collision. Large coherent continental masses were extruded along major strike-slip shear zones, accounting for much of the intracontinental deformation, which finally resulted in the current structural geometry of southeastern Asia (Fig. 1a; Leloup et al., 2001; Morley, 2007; Searle et al., 2010). The Ailao Shan–Red River, Biluoxueshan–Chongshan, and Gaoligong–Sagaing faults are regional-scale strike-slip faults that extend to the northwest into Tibet (Fig. 1a). The Ailao Shan–Red River fault zone consists of an NW–SE-trending zone of variably mylonitized metamorphic and igneous rocks that underlie part of the Xuelong Shan, Diancang Shan, and Ailao Shan metamorphic massifs in Yunnan (Leloup et al., 1995, 2001; Wang and Burchfiel, 1997; Zhang and Schärer, 1999; Searle, 2006; Zhang et al., 2006). To the west lies the Gaoligong fault zone (Fig. 1), another regional-scale fault bordering the Eastern Himalayan Syntaxis (EHS).

Along with other large-scale strike-slip faults (the Karakoram and Jiali faults) in Tibet (Lee et al., 2003), the Gaoligong fault zone has been proposed as evidence for large-scale extrusion of Tibetan and southeast Asian continental crust away from the Indian plate indenter in the Tertiary (Ding, 1991; Wang and Burchfiel, 1997; Ji et al., 2000; Leloup et al., 2001; Tapponnier et al., 2001). Early studies of the Gaoligong fault zone identified a stage of ductile, dextral strike-slip deformation based on structures in mylonite along the eastern flank of the Gaoligong mountains (Ding, 1991; Zhong, 2000). High-grade metamorphism and granite melting along the Gaoligong shear zone is Tertiary in age (Song et al., 2010); U–Pb ages of zircon in granite yield the timing of strike-slip shear

* Corresponding author.
E-mail address: geozhangbo@pku.edu.cn (B. Zhang).

0191-8141/$ – see front matter © 2012 Elsevier Ltd. All rights reserved.
doi:10.1016/j.jsg.2012.02.007

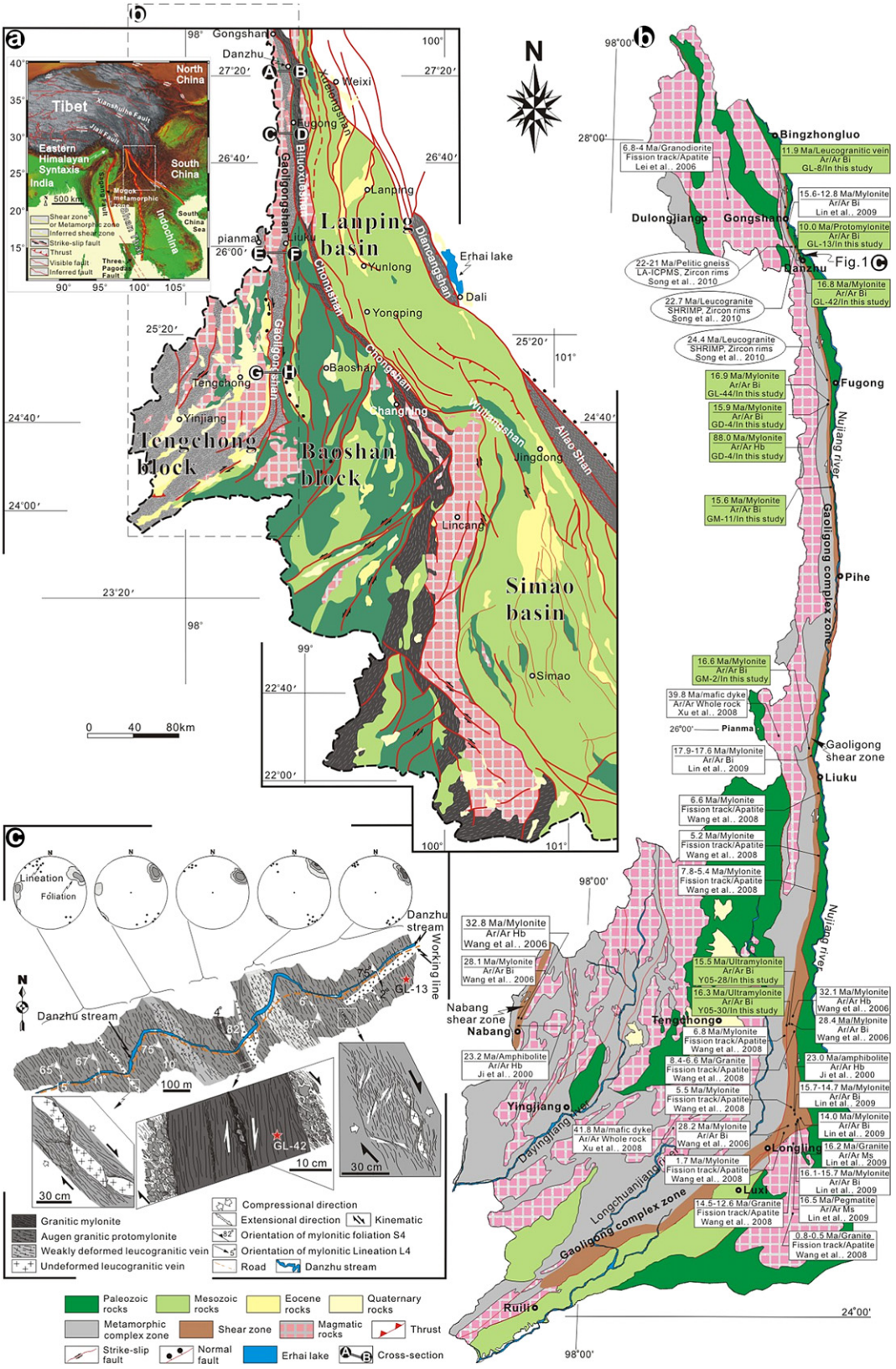

Fig. 1. (a) Simplified structural map of southwestern Yunnan, showing major lithological units, including the Tengchong, Baoshan, and Lanping Simao basins, and the Gaoligong, Chongshan, and Xuelong Shan–Diancang Shan–Ailao Shan zones (modified from the geological map of Yunnan, scale: 1:500,000; Wang and Burchfiel, 1997; Wang et al., 2008). The inset map shows topographic and major tectonic features of southeastern Asia and adjacent areas, including major faults systems and metamorphic zones (modified from Leloup et al. (1995), Wang and Burchfiel (1997), Zhang and Schärer (1999), Tapponnier et al. (2001), Lee et al. (2003), Searle (2006), Zhang et al. (2010)). (b) Detailed geological map of the Gaoligong zone and adjacent region with geochronological data from previous studies (Ji et al., 2000; Lei et al., 2006; Wang et al., 2006; Wang et al., 2008; Xu et al., 2008; Lin et al., 2009; Song et al., 2010) and from this study. (c) Detailed structural map of mylonite outcrops within the Gaoligong ductile shear zone, showing inhomogeneous strain, and kinematics along the Danzhu stream west of Danzhu (27°37.679′N; 98°40.437′E; elevation: 2060 m) (location of the map is shown in Fig. 1b). The stereonets (lower hemisphere, equal-area projections) show foliation (S4) and lineation (L4) orientations across the shear zone.

(Ji et al., 2009; Lin et al., 2009). Recent field-based studies of metamorphic rocks have revealed evidence for older ductile events (Song et al., 2010).

Major controversies surround the timing of deformation, scale, and role of large-scale continental strike-slip faults in continental extrusion (e.g., Wang and Burchfiel, 1997; Wang et al., 1998; Zhong, 2000; Jolivet et al., 2001; Leloup et al., 2001; Gilley et al., 2003; Searle et al., 2010). Two end-member models predict significantly different mechanisms to explain crustal deformation in the EHS region. One school of thought advocates an essentially rigid indentation–extrusion model where deformation is localized along major strike-slip faults that penetrate to the mantle; mantle-derived magmas were extruded into shear zones at ca. 35 Ma (Tapponnier et al., 1982, 2001; Leloup et al., 1995; Wang et al., 2006). The alternative viewpoint contends that a mid-crustal high-temperature layer of partially molten rock existed, and separated the brittle upper crust from the granulite–eclogite lower crust. As a result, strike-slip faults were confined to the upper crust, failing to penetrate to more ductile regions, terminating with increasing depth somewhere in the middle or lower crust (e.g., Jolivet et al., 2001; Shen et al., 2005; Morley, 2007; Searle et al., 2010).

To assess the validity of these models, it is necessary to perform field-based structural analyses of the major metamorphic units around the EHS. As the largest and most continuous representative basement exposure in the EHS region, the Gaoligong metamorphic zone is the best target for a study aimed at understanding the structural architecture and crustal deformation processes in this region. Of particular significance is the presence of greenschist facies mylonite, migmatite, high-grade metamorphic gneiss, and leucogranite (Socquet and Pubellier, 2005; Wang et al., 2006). Recently, Li et al. (2008) and Zhang and Wang (2009) carried out magnetotelluric (MT) geophysical profiling along the southernmost segment of the Gaoligong zone in the Longling–Ruili area. These studies indicate the existence of a sub-horizontal detachment within a conductive mid-crustal layer at a depth of ~10 km that was apparently not significantly affected by faulting (Bai and Meju, 2003). It is important to note that a comparable crustal boundary was identified in the Gaoligong, Chongshan, and Ailao Shan–Red River regions using wide-angle seismic tomography (Huang et al., 2009; Zhang and Wang, 2009); it has been suggested that intra-crustal detachments exist in these areas (Zhang and Wang, 2009). Geophysical studies were limited to deep crustal levels, and thus are insufficient for understanding the entire structural evolution of the Gaoligong zone.

In the present study, we have synthesized data from field-based structural observations, microstructural investigations, analyses of crystal preferred orientations (CPOs), and $^{40}Ar/^{39}Ar$ geochronological studies in the Gaoligong zone. On the basis of the available information, we present new assessments of the kinematic evolution of the metamorphic zone. Combining our new structural data with known conditions of metamorphism, leucogranitic emplacement setting, and cooling ages, we discuss the possible tectonic mechanisms that led to the present-day geometry of the EHS region.

2. Geological overview of the Gaoligong zone

The Gaoligong zone is a narrow N–S-trending belt, ~10 km in width and 600 km in length, that defines a discontinuous intracontinental boundary in southeastern Asia (Fig. 1b). Southward, the zone merges with the Sagaing Fault in Burma, dipping north into the EHS (Fig. 1a; Wang and Burchfiel, 1997; Ji et al., 2000; Lin et al., 2009). The zone forms the boundary between the Tengchong–Burma and Baoshan blocks, and is characterized by a large-scale first-order antiform that is bound by the sub-vertical Gaoligong shear zone to the east (Fig. 1b; BGMRYP, 1990). The shear zone is truncated by a brittle, dextral fault along the east side of the Gaoligong mountains (Wang et al., 2008). The zone can be further divided into granitoid and high-grade gneiss units (Fig. 1b).

In the western part of the Gaoligong mountain chain, the granitoid unit (Fig. 1b) has been named the Gangdese batholith, interpreted as an Andean-type magmatic arc preserved in the Lhasa and east Burma–Tengchong blocks, which resulted from the northward subduction of the Neotethyan slab (BGMRXZR, 1993; Lee et al., 2003; Ji et al., 2009). Gaoligong granite batholiths are dominated by medium- to fine-grained, undeformed to weakly foliated, peraluminous to strongly peraluminous leucogranites and granodiorites. Provenance studies yielded negative $\varepsilon_{Hf}(t)$ values (−12 to −4) for zircon, indicating a Proterozoic sedimentary source (Xu et al., 2008). Recent U–Pb zircon analyses show that the Gaoligong granitic protolith was emplaced in four discrete stages of magmatic activity: Early Paleozoic (502–498 Ma; Chen et al., 2006; Song et al., 2010), Triassic (259–200 Ma; Chung et al., 2005; Song et al., 2010), Cretaceous (140–70 Ma, Chen et al., 2006; ca. 90–80 Ma, Chung et al., 2005), and Tertiary (Fig. 1b; ca. 65–41 Ma and ca. 33–13 Ma, with the 65–41 Ma stage being the most prominent as reported by Chung et al. (2005) and Ji et al. (2009)). Cenozoic magmatism is suggested to correspond with crustal thickening resulting from partial melting of the thickened lower crust, impinging the base of the crust (Xu et al., 2008; Chung et al., 2009).

The high-grade gneiss unit, referred to as the Gaoligong Group (Fig. 1a, b; BGMRYP, 1990; Zhong, 2000), has long been described as Precambrian basement that experienced high-grade metamorphism. Recent studies indicate that the Gaoligong Group was reworked during the Tertiary to form the Gaoligong ductile shear zone along its eastern side (Ding, 1991; Wang et al., 2006). High-grade gneisses are low-pressure, high-temperature pelitic migmatites consisting of amphibolite, migmatite, garnet–biotite–sillimanite gneiss, marbles, and garnet-bearing leucogranite veins. Paragneiss and orthogneiss are dated at 1053–635 Ma and 490–470 Ma, respectively, corresponding to the Neoproterozoic and Mesozoic (Song et al., 2010). The gneisses consist mainly of migmatite and pelitic paragneiss with well-defined mineralogical banding. The metamorphic history of the Gaoligong Group complex has been described for metapelite (Song et al., 2010) and pelitic gneisses (Ding, 1991; Ji et al., 2000; Zhong, 2000; Song et al., 2010). Three distinct metamorphic stages were identified from the Gaoligong gneisses (Fig. 2b; Ding, 1991; Zhong, 2000): medium to high-pressure (M1), peak (M2), and late cooling and retrogression (M3 and M4). M1 metamorphism formed the kyanite + staurolite + sillimanite + plagioclase + quartz + biotite + muscovite assemblage at conditions of 7.0–7.5 kbar and 600–650 °C (Ding, 1991; Zhong, 2000). Peak metamorphism (M2) is characterized by mineral assemblages consisting of garnet porphyroblasts with plagioclase + quartz + biotite at P–T conditions of 6.5–7.0 kbar and 700–750 °C (Ding, 1991; Ji et al., 2000; Zhong, 2000). Late cooling and retrogression (M3 and M4) developed epidote + chlorite + plagioclase + muscovite assemblages at P–T conditions of 4–5 kbar and 500–600 °C (Ding, 1991; Zhong, 2000). The reconstructed P–T path shows a clockwise trajectory that is characterized by early near-isobaric heating and late decompression and cooling (Fig. 2b). In Fig. 2a the trajectory proposed by Song et al. (2010) is shown for comparison, indicating a two-stage P–T path for metapelites and pelitic gneisses, although at higher P–T conditions than those reported by Ding (1991) and Zhong (2000). Petrographic observations and thermobarometric estimates revealed an early stage of amphibolite facies metamorphism (650–660 °C and 7.1–8.3 kbar; 685–750 °C and 6.5–8.4 kbar; Song et al., 2010), and late greenschist facies cooling and retrograde metamorphism (Song et al., 2010; Fig. 2a). The P–T paths described above suggest that the Gaoligong complex is the result of a tectonothermal process that featured an initial period of crustal thickening followed by exhumation and cooling (Zhong, 2000; Song et al., 2010).

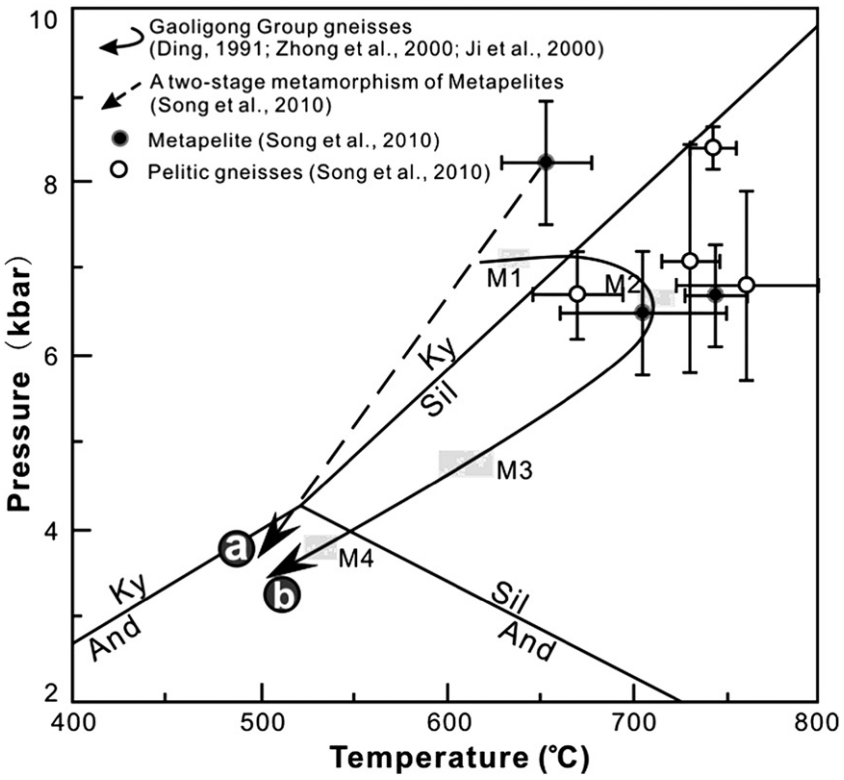

Fig. 2. Metamorphic P–T paths of the Gaoligong massif. (a) P–T path for metapelites from Carboniferous strata, showing two-stage metamorphism (note: four samples of the Gaoligong Group metapelitic gneisses record the conditions of anatexis via a muscovite dehydration reaction) (Ji et al., 2000; Song et al., 2010). (b) P–T path of the Gaoligong Group gneiss (Ding, 1991; Zhong, 2000; Wang et al., 2006).

The Gaoligong shear system is an N–S trending dextral quartzo-feldspathic mylonite zone with a width of 1–5 km. It extends from the EHS to the Longling–Ruili area, and then bends to the northeast to link with the Sagaing Fault in Burma (Fig. 1a, b, Wang and Burchfiel, 1997; Morley, 2007). Its northern segment intersects two major branches of the Jiali shear zone (the Poqu and Parlung faults) in Tibet (Fig. 1a, Lee et al., 2003; Lin et al., 2009). Wang and Burchfiel (1997), Wang et al. (2006), and Socquet and Pubellier (2005) discussed the structural evolution of the southern segment of the Gaoligong shear zone where a steeply dipping metamorphic foliation and associated sub-horizontal mineral stretching lineation have developed along the Gaoligong mountain chain. Morley (2007) and Socquet and Pubellier (2005) have suggested that the shear zone is a late Tertiary transpressional deformation zone.

Recent geochronological studies have revealed that the shear zone experienced a major tectonothermal episode in the Tertiary (Fig. 1). Current geomorphologic and geodetic data show the Gaoligong shear zone to be a dextral strike-slip fault zone (Shen et al., 2005). Zhong (2000) and Ji et al. (2000) have reported right-lateral strike-slip shearing motion occurred at 24–19 Ma and 14–11 Ma on the basis of hornblende and plagioclase $^{39}Ar/^{40}Ar$ plateau and isochron ages. However, Akciz et al. (2003) state that right-lateral movement in the zone ended at ca. 18 Ma, based on mica argon plateau ages in granitoid gneiss and leucogranite. The main dextral shearing event evident along the zone's northern segment, as it crosses into the Pulung–Jiali fault zone, has been constrained to the period 18–12 Ma on the basis of $^{39}Ar/^{40}Ar$ isochron ages of mica in mylonites (Lee et al., 2003; Lin et al., 2009). Syn-tectonic mica $^{39}Ar/^{40}Ar$ plateau ages from the zone's southern segment range from 32 to 22 Ma (Wang et al., 2006). According to Lin et al. (2009), Miocene ductile strike-slip shearing is characterized by metamorphic conditions of ~550 °C and 3–5 kbar (Fig. 2). This major, right-lateral, ductile strike-slip shear is considered responsible for the uplift and exhumation of the Gaoligong complex high-grade gneisses (Wang et al., 2006; Morley, 2007). Socquet and Pubellier (2005) and Wang et al. (2008) documented that the transition from ductile–dextral to brittle–sinistral settings in the Gaoligong, Nabang, and associated N–S faults with normal dip–slip components probably post-dates 11 Ma (i.e., likely occurred in the Middle–Late Miocene or more recently).

3. Structural evolution

The Gaoligong zone is characterized by the folding and shearing that record the Cenozoic and pre-Mesozoic tectonic evolution of southeastern Asia. Both the Gaoligong unit and Baoshan block were affected by deformation in the Gaoligong zone. In order to determine its structural geometry, four cross-sections were constructed across the Danzhu, Fugong, Pianma, and Tengchong regions. Based on overprinting and geometric relationships, four stages of deformation were identified, corresponding to four sub-domains (Table 1; Fig. 3; D1–D4). Although structural fabrics display varying degrees of geometric and kinematic complexity (Figs. 3 and 4), they record a progressive transition from early ductile deformation (D1–D3) associated with peak metamorphism, through ductile to ductile–brittle strike-slip shear deformation (D4) associated with exhumation. Domains D2, D3, and part of D1 (Fig. 3) are situated on the western side of the zone, which experienced significant deformation as folding. The D4 domain and part of D1 preserve dextral ductile shear zones and F1 folds, which are typically located on the eastern side of the zone (Fig. 3). The early deformation stages (D1 and D2) involved the formation of folds in the D1 and D2 domains. Younger folding (D3) resulted in the major

Table 1
Structural features of D1–D4 deformation in the Gaoligong zone.

Stage	Location	Major structure	Scale	Mineral assemblage	Strain pattern
D1	In D1 domain in metamorphic Paleozoic rocks	Tight to isoclinal fold F1, foliation S1 trending along N-S, and NWN-SES	Megascopic, mesoscopic	Gt + Stl + Ky + Bi + Ms + Pl + Qz	Shortening
D2	In D2 domain in Gaoligong gneiss	Recumbent F2, Sub-horizontal axial planes, Sub-horizontal stretching lineation	Mesoscopic, macroscopic, microscopic	Gt + Stl + Ky + Bi + Ms + Pl + Qz	Horizontal shearing
D3	In D3 domain in Gaoligong geniss	Upright fold F3 with nearly N-S, NWN-SES trending, Sub-horizontal stretching lienation	Megascopic, mesoscopic	Gt + Stl + Ky + Bi + Ms + Pl + Qz	Shortening with dextral shearing
D4	In D4 domain in mylonitic gneiss	Vertical and sub-vertical mylonitic foliation, sub-horizontal stretching lineation, deformed leucogranitic veins	Mesoscopic, macroscopic, microscopic	Qz + Bi + Ms + Chl	Dextral strike-slip shearing

Gt: garnet, Stl: staurolite, Ky: kyanite, Bi: biotite, Ms: muscovite, Pl: plagioclase, Qz: quartz, Chl: chlorite.

dome-shaped antiformal zone along the D3 domain within the main massif. Shearing and exhumation occurred in the D4 domain during the youngest deformation event in the Gaoligong zone.

3.1. D1 deformation

D1 structures were reoriented during subsequent deformation events. The current orientations of D1 structures and interference patterns formed during later events vary widely. The simplest structures are isoclinal F1 folds that have been intensely deformed during D3 and D4.

In the field, D1 is observed as folds that are only preserved in outcrops of Paleozoic metasedimentary rocks (Figs. 3 and 5a) and in some Gaoligong gneisses from the Gongshan, Dulongjiang, and northern Gongshan regions (Fig. 5a). Structures designated as D1 are macroscopic to large-scale, tight to isoclinal upright folds (F1) with predominantly NW–SE-striking axial planes resulting from a folding event (Figs. 4, 5b, d). S1 foliations associated with D1 fabrics are penetrative planar foliations or spaced cleavages that strike between 000° and 034°, and dip variably to the east or west (Fig. 4). Original sedimentary bedding, S0, is rarely discernable. S1 is defined by compositional layering, the preferred orientation of platy minerals in metasedimentary rocks and amphibolites, foliation-parallel garnet-bearing leucogranite pods and veins, and the preferred orientation of biotite in granitoid migmatites (Song et al., 2010). In migmatized gneiss, S1 is defined by curved felsic ribbons and aligned biotite. Regionally, S1 foliations exhibit moderate to steep dips and variable strike orientations due to later deformation events (Figs. 3 and 5d). In localities where S1 is completely overprinted by subsequent deformation (Fig. 5b, d; D3 and/or D4), the stretching lineation observed on fold limbs usually represents L2 or L3. Although S1 foliations have been folded to various orientations, an SW–NE contraction may be inferred (Fig. 4).

Some D1 domain metapelite is coarse-grained with garnet + staurolite + kyanite + biotite + muscovite + plagioclase + quartz mineral assemblages indicating granulite facies conditions for D1 (Ji et al., 2000; Song et al., 2010).

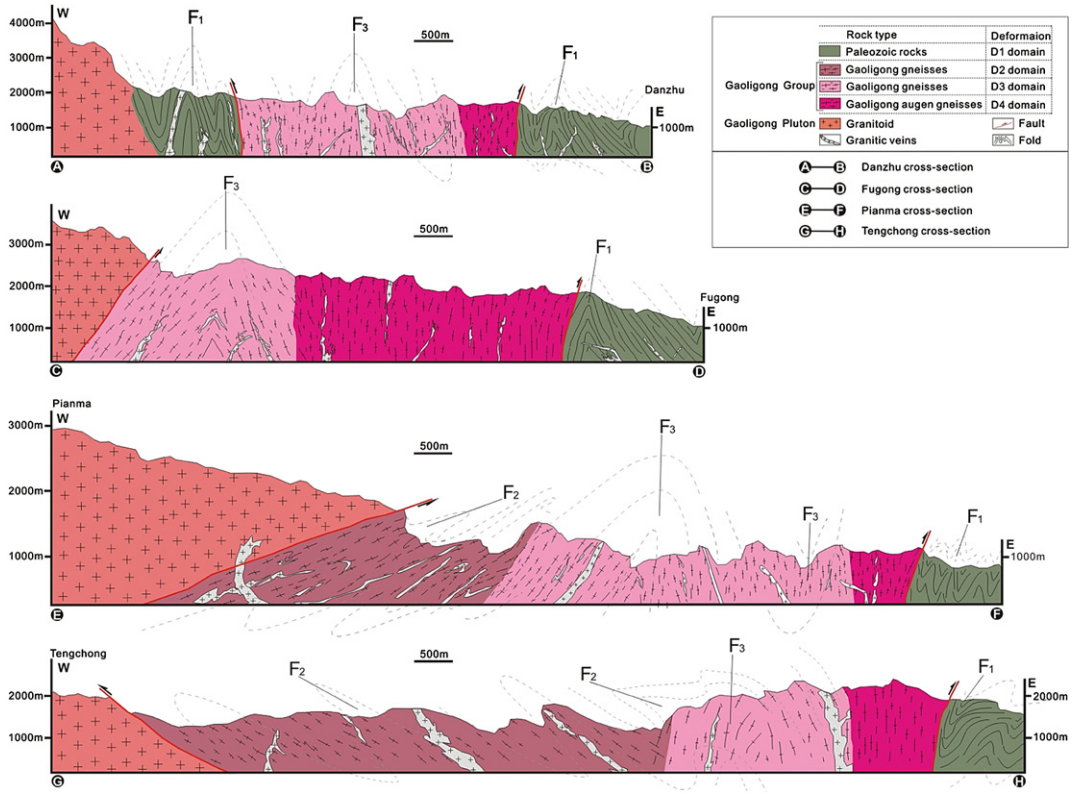

Fig. 3. Cross-sections of the Gaoligong metamorphic zone, highlighting the various structural domains.

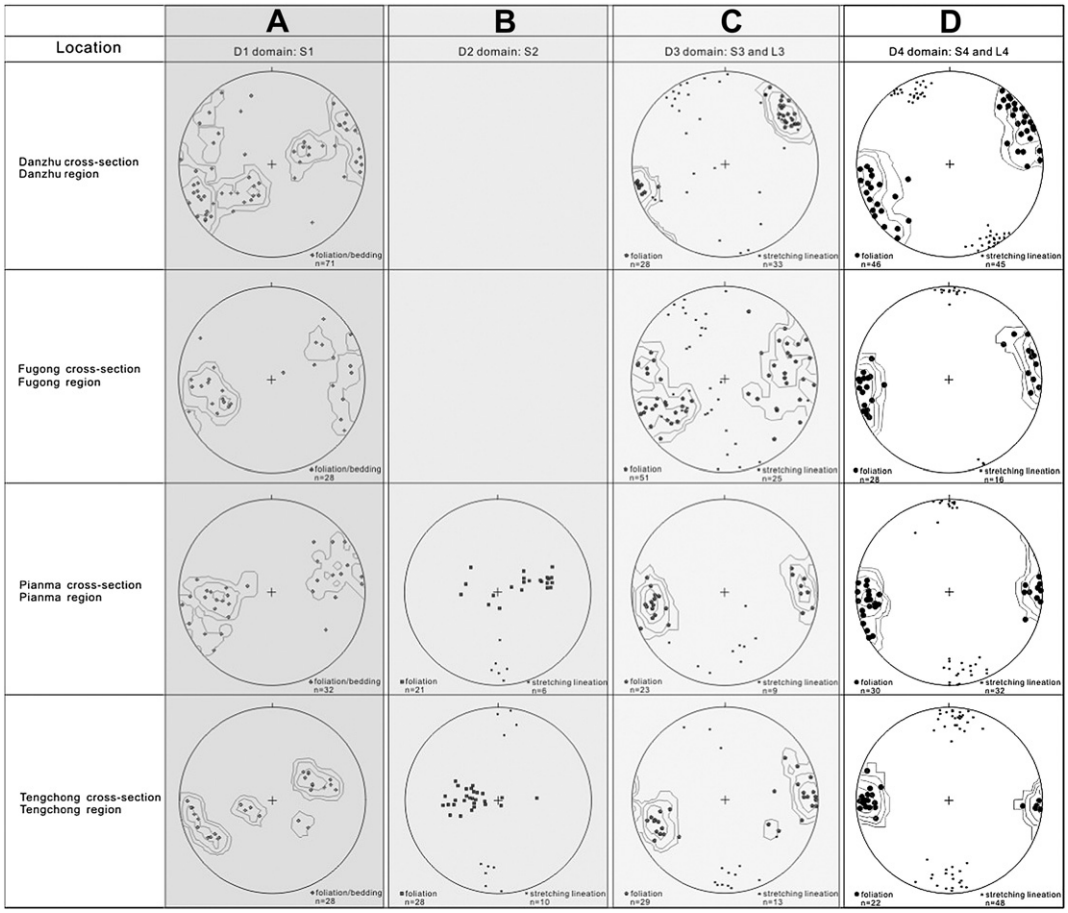

Fig. 4. Stereonet plots (lower hemisphere, equal-area projections) showing the orientations of D1–D4 fabrics in different domains of the Gaoligong metamorphic zone. (A) Schist foliation and bedding in metamorphic Paleozoic rocks affected by D1. (B) Gneiss foliation and stretching lineation in Gaoligong gneiss and migmatized gneiss affected by D2. (C) Gneiss foliation and stretching lineation in Gaoligong gneiss affected by D3. (D) Mylonitic foliation and stretching lineation in a ductile shear zone affected by D4.

3.2. D2 deformation

Intense shortening at several locations within the study area is associated with D2. It is manifested as tight, asymmetric, or recumbent folds (F2) at different scales observed in most D2 domains in the Gaoligong gneiss zone (Figs. 3, 4 and 5b, c, e, f). Although D2 structures were overprinted by D3 folds, D2 and D3 fabrics are easily distinguished at various scales in outcrop. We performed a detailed structural investigation to determine the key characteristics of D2 deformation and its relationship to D1 and D3 events (Figs. 3 and 5d–f). Refolded sub-horizontal isoclinals folds (F2) with sub-horizontal to shallow-dipping axial planes (S2) bear a sub-horizontal stretching lineation parallel to the strike of the zone (Fig. 4). The S2 foliation is defined by compositional layering and the preferred orientation of platy minerals in gneisses and amphibolites, and by the preferred orientation of biotite in granitoid migmatites. In orthogneisses, S2 is characterized by the development of quartz and feldspar ribbons (Fig. 5b, e, f). S2 foliations generally display shallow dips (Fig. 5d), which become much steeper at localities that were affected by upright and open folding during D3 (Figs. 3 and 5e, f). The dip orientation of S2 varies between E and W due to later refolding (Pianma section and Tengchong section in Fig. 3). At localities with intensely developed folds of S2, it is not clear whether the lineation observed on fold limbs is L2 or L3.

Numerous mafic boudins and metapelite lenses outcrop in the D2 domain of the Gaoligong gneiss zone. Some of these can be traced over several tens of meters along their length, suggesting they were derived from mafic dykes and anatexis (Song et al., 2010). Dykes and lenses are boudinaged and rotated into parallelism with S2 in enclosing gneisses (Fig. 5e). Petrographic analyses show that metapelite lenses are composed of coarse-grained mineral assemblages of garnet + sillimanite + kyanite + biotite + muscovite + plagioclase + quartz (Song et al., 2010). Our observations suggest that pre-existing metapelite layers experienced intensive stretching, shearing, and granulite-facies metamorphism under anatectic conditions during D2 deformation.

3.3. D3 deformation

D3 deformation fabrics are characterized by large-scale antiforms (Fig. 3). The eastern limb of the kilometer-scale antiform is overprinted by ductile shearing in the Gaoligong shear zone. Well-developed ductile D3 fabrics are characterized by large-scale F3 folds that cross-cut or refold earlier D1 and D2 fabrics (Figs. 3 and 5d–f). For the most part, F3 folds are large-scale tight folds with a penetrative axial planar S3 foliation (Fig. 6a, b). F3 fold axes generally trend NNW–SSE, similar to F1 fold orientations though not F2 (Fig. 4). The superimposition of F3 on F2 resulted in the regional doming pattern (Fig. 3). The regional F3 folding domain (i.e., the D3 domain) formed the Gaoligong Group gneiss cores and reflects compressional deformation. F3 folds commonly have sub-vertical axial planes with moderately NNW-plunging fold axes, parallel to L3 and newly developed L4 lineations (Fig. 4). The domain preserving D1 and D2 features is sharply bound by a penetrative sub-vertical S3 foliation that dominates the entire eastern part of the zone (Fig. 3).

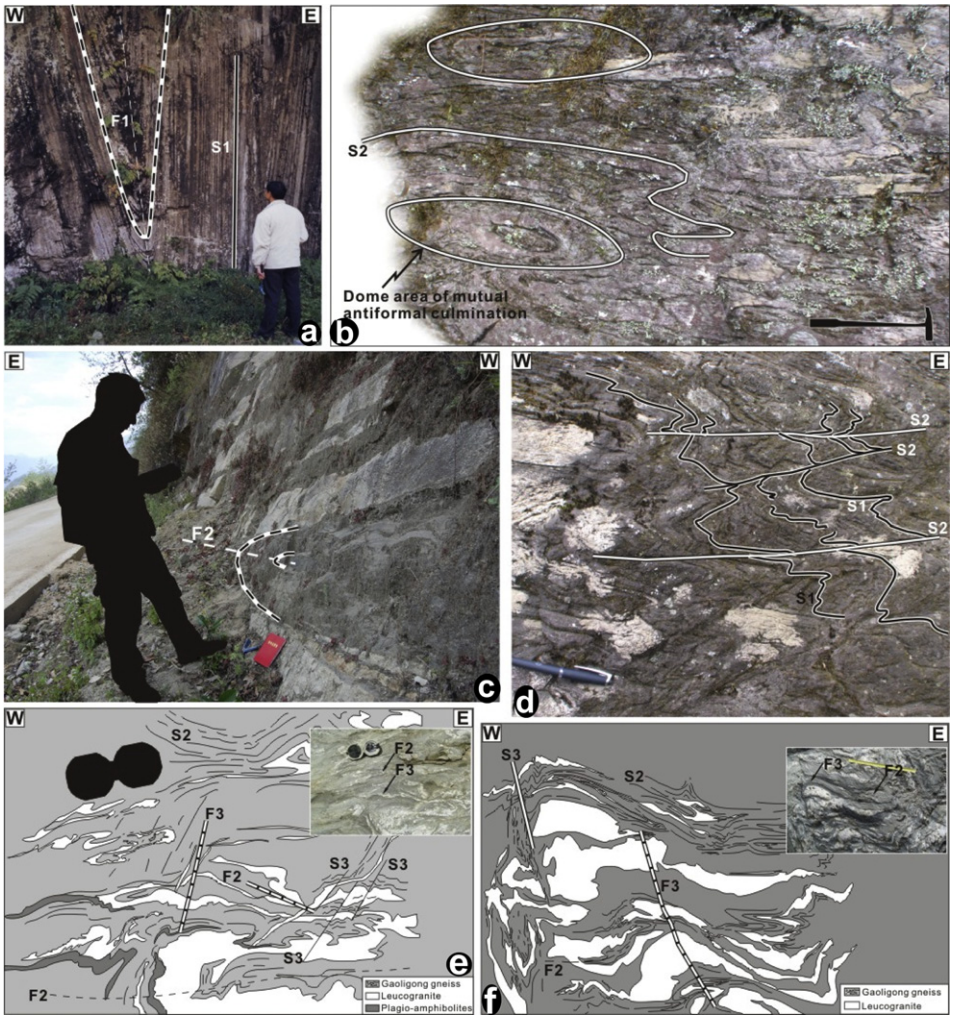

Fig. 5. Field photographs showing typical fabrics associated with D1–D3. (a) F1 vertical isoclinal folds preserved in metasedimentary rocks. (b) F1–F2 fold interference patterns in metasedimentary rocks in northern Gongshan (observed on the *YZ*-plane), similar to "dome and basin" type I interference patterns resulting from two successive folding events (Ramsay and Lisle, 2000). (c) East-verging meso-scale recumbent F2 folds with horizontal fold axial planes in Pianma section gneiss. (d) Overprinting relationship between S1 and S2 preserved in paragneiss in the Gongshan–Dulongjiang region (observed on the *YZ*-plane). (e) Sketch of the outcrop photograph, showing the overprinting relationship between F2 and F3 folds near the Fugong region (observed on the *YZ*-plane). (f) Strongly deformed Gaoligong gneiss, showing F3 folds overprinting F2, where F3 isoclinal folds have transposed the S2 foliation into S3 (observed on the *YZ*-plane).

Gaoligong gneisses dominate the D3 domain, and gneissic fabrics are predominantly attributed to D3 deformation. However, the intensity of D3 deformation varies considerably between the various cross-sections (Fig. 3). The style of deformation varies: some areas are characterized by F3 fold structures with sub-vertical, usually NW–SE-striking axial planes as in the Danzhu and Tengchong sections (in Fig. 3), while other areas are characterized by nearly N–S-striking axial planes with north- or south-plunging lineations, as in the Pianma and Fugong sections (Fig. 3). Some D3 features were observed in the Longling–Luxi region Gaoligong gneiss (BGMRYP, 1990).

We interpret the fabrics of the gneiss antiform as the result of D3 having been superimposed on an early, shallow-dipping D2 fabric (Fig. 5e, f). The western limb of the antiform may represent an early D2 fabric that was rotated and shortened during D3.

The Gaoligong gneiss and leucocratic veins surrounding mafic boudins were warped by F3, as shown in Fig. 6b, in the Tengchong–Luxi region (seeing also Zhong (2000); p. 191, Figs. 7–12). In F3 hinge zones, anatectic felsic veins and dykes commonly occur oriented co-planar with S3 cleavages (Figs. 3 and 5f), suggesting that D3 was associated with partial melting during decompression and exhumation (M3 stage; Ding, 1991).

3.4. D4 deformation

After D3, the style of deformation changed from one where folding predominated to one of ductile strike-slip shearing, defining the D4 shear zone domain and associated ductile features. N–S-trending ductile shear zones generated large-scale ductile shear structures that dominate the entire eastern side of the Gaoligong massif. The most well-known examples of D4 features occur in this area, which are typically steep to sub-vertical mylonitic foliations (Figs. 3, 4, 6c–g).

The D4 domain is characterized by mylonites that tectonically rework and overprint other Gaoligong lithologies and structures (Figs. 6c–g, 7, 8) including S2 gneiss foliations, F2 fabrics, Paleozoic S1 foliations, and F1 fabrics (Fig. 3). The domain interior is characterized by a pervasive, N–S-striking foliation, with a shallowly plunging (1°–20°) mineral stretching lineation (Figs. 4, 7f–h). The mylonitic foliation is defined principally by quartz ribbons and the preferred orientation of biotite and muscovite. The strong variation in mylonitic fabrics and types suggests that significant differences in temperature and strain existed within and across the mylonite zone (Figs. 7 and 8). To the west, domains with preserved D3 structures are overprinted by a penetrative sub-vertical S4 foliation,

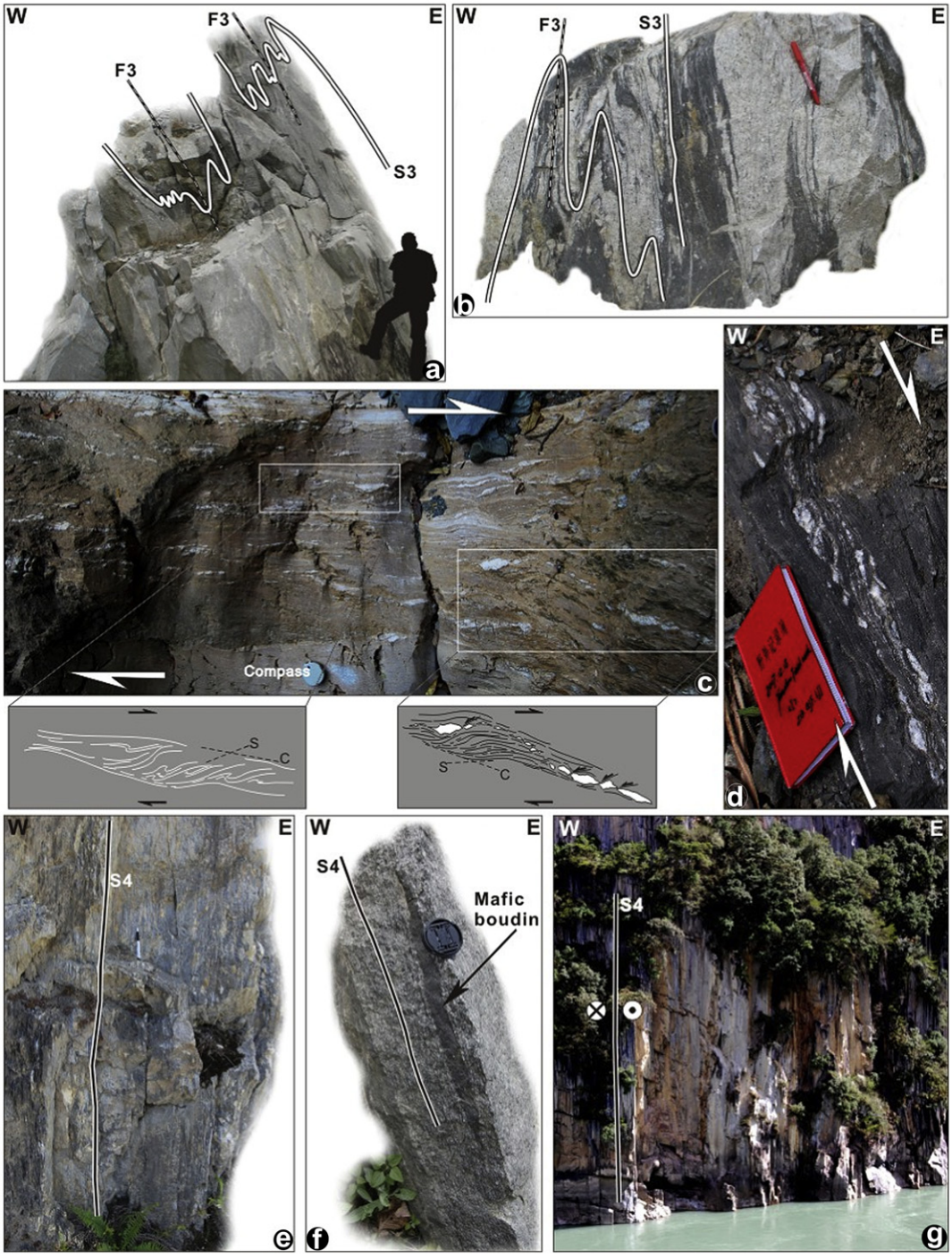

Fig. 6. Field photographs showing typical fabrics associated with D3 and D4. (a) Tight to isoclinals F3 folds with sub-vertical axial planar S3 developed in high-grade garnet-bearing metapelite of the Gaoligong gneiss near Gongshan (observed in the *YZ*-plane). (b) Garnet-bearing leucogranitic bands and pelitic gneiss deformed to form tight F3 folds (observed in the *YZ*-plane) in the Fugong region. (c–d) Mylonitic marble with calcite and quartz boudins along the S4//S1 foliation on the east side of the Gaoligong shear zone in the northern part of the zone (observed in the *XZ*-plane). (e) Sub-vertical S4 foliation in mylonitized granite, with feldspar boudins along the S4 foliation (observed in the *YZ*-plane). (f) Mafic boudin parallel to S4, hosted in mylonitic granodiorite (observed in the *YZ*-plane). (g) Vertical mylonitic foliation in fine-grained leucogranite with a penetrative S4 foliation (observed in the *YZ*-plane) in northern Gongshan.

and moderate to steeply dipping F3 cleavages have been steepened to near vertical because of shearing (Fig. 3). This observation suggests that for the most part, the Gaoligong ductile shear zone formed after D3 deformation. L4 lineations associated with the mylonitic foliation are sub-horizontal, north- or south-dipping quartzo-feldspathic mineral stretching lineations (Figs. 4 and 7g, h). Kinematic indicators (e.g., S–C structures, drag folds, and asymmetric porphyroblasts) in the ductile shear zone show predominantly dextral asymmetries related to strike-slip movement (Figs. 1c, 7a–f, 8a–d).

The development of a sub-vertical S4 foliation coincided with the formation of foliation-parallel leucosome in mylonite (Fig. 7b, e). Leucosomes form long bands that are locally connected by melt-filled shear bands (Fig. 1c). D4 tectonites vary from S–C mylonites to coarse-grained augen gneisses (Fig. 7c, d). Most of the sedimentary bedding and secondary foliations in the eastern quartzites

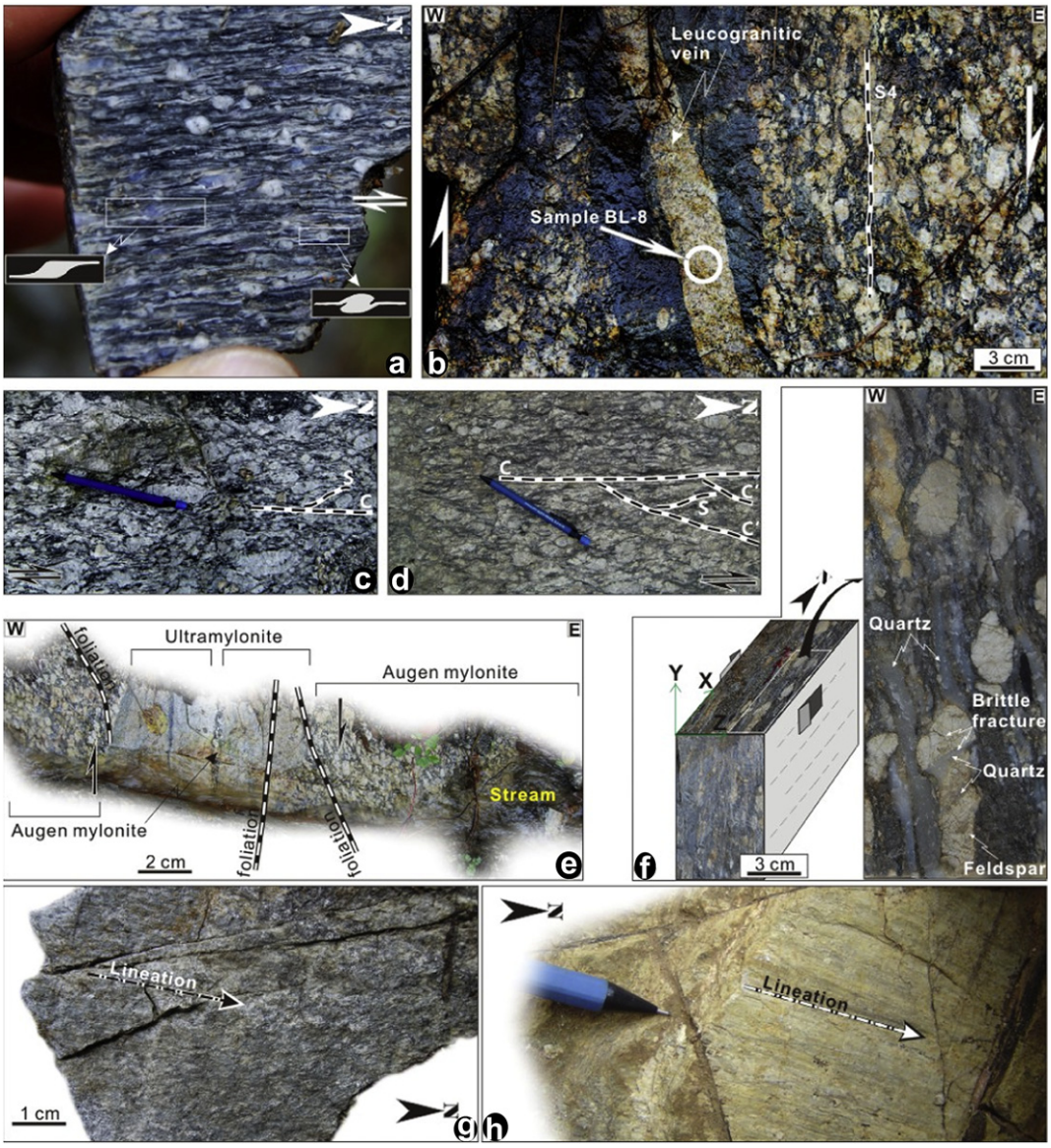

Fig. 7. Field photographs showing typical structures and fabrics associated with D4 ductile shearing. (a) Augen granitic mylonite with σ- and δ-type porphyroblasts indicating dextral shearing (sample GL-44, observed in the *XZ*-plane). (b) Weakly deformed fine-grained leucogranitic vein (sample BL-8) showing a weak foliation sub-parallel to the host augen granite protomylonite affected by D4 deformation (observed in the *XZ*-plane), northern Gongshan. (c–d) Strongly deformed coarse-grained granitic mylonites showing penetrative S–C fabrics and spaced C′-planes indicate dextral shearing (observed in the *XZ*-plane). (e) Thin leucogranitic ultramylonite vein with a penetrative foliation oriented sub-parallel to the foliation in the coarse-grained augen granitic mylonite host, indicating that its emplacement was syntectonic and that strain partitioning between the vein and the host occurred during D4 deformation (observed in the *XZ*-plane). (f) Strongly deformed coarse-grained granitic mylonite in three-dimensional space, showing stretched and flattened feldspar and quartz grains in the *YZ*-plane and *XZ*-planes, respectively. (g) Sub-horizontal mineral stretching lineations upon the foliation in granitic mylonite. (h) Sub-horizontal mineral stretching lineation in the foliation of fine-grained ultramylonite.

and mica schists within the D1 domain have a strike that is parallel to the orientation of the shear zone (Fig. 6c, d), reflecting a strong reorientation during D4.

The effects of D4 are more significant in other domains, particularly where all previous structures have been reoriented or rotated. In such cases, the final structures are polyphasic with composite D1–D4 structures reoriented and tightened during D4. D4 stretching lineations associated with dextral shearing plunge shallowly to the north or south (Fig. 3), while D3 lineations plunge orientations are variable in the Danzhu region, south-plunging in the Pianma region, gently south- or north-plunging in the Fugong region, and predominantly south-plunging in the Tengchong region. Therefore, it is possible to discriminate between D3 and D4 on the basis of deformation style and the orientation of the stretching lineation. Anatectic felsic veins and dykes commonly occur along the S4 foliation in the D4 domain (Fig. 7b, e) and are more or less oriented parallel to the host mylonite foliation.

The ductile shear zone was reactivated during subsequent brittle deformation and resulted in the overprinting of D4 ductile shear features by brittle and semi-brittle ones. The widespread development of meso- to regional-scale high-angle strike-slip faults with a normal dip-slip component is related to the brittle deformation (Socquet and Pubellier, 2005; Wang et al., 2008). Similar brittle structures are observed in the Gaoligong granitic pluton and ductile shear zone, and are interpreted as exhumation-related collapse structures (Socquet and Pubellier, 2005; Wang et al., 2008).

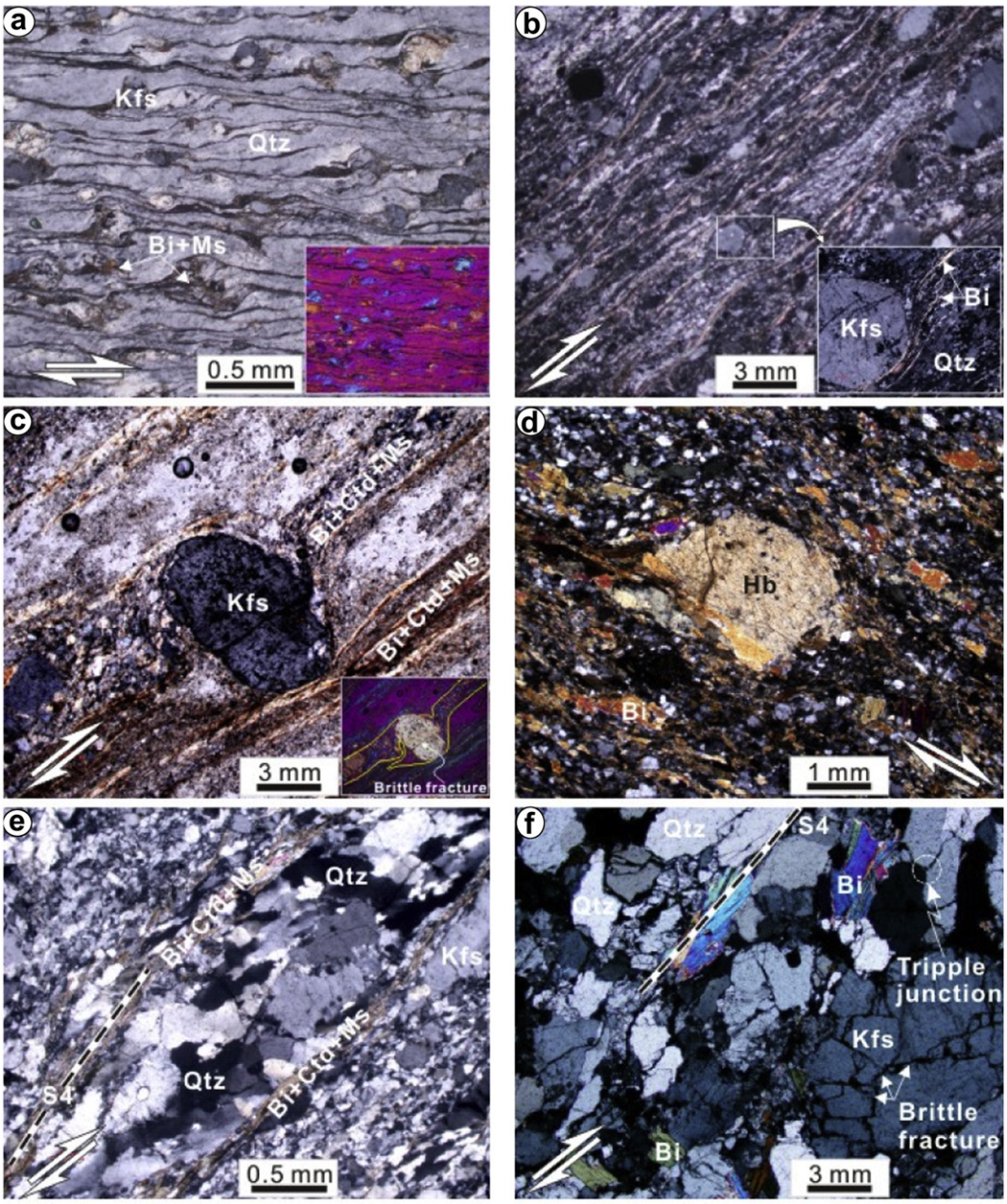

Fig. 8. Photomicrographs of various deformed rocks. (a) Asymmetric K-feldspar porphyroclast (σ-type) and quartz ribbons in an oriented thin section, from sample GL-44. (b) Asymmetric K-feldspar and quartz porphyroclast (σ- and δ-type) in sample GL-44 from the augen granite mylonite. (c) δ-type K-feldspar porphyroclast showing that in-plane tails adjacent to the microcline porphyroclast were deflected, indicating dextral shearing in the granitic ultramylonite. (d) σ-type porphyroclast of hornblende with asymmetric tails showing that fine-grained quartz, biotite, hornblende, and feldspar matrix grains define S4. (e) Polycrystalline quartz bands that probably developed predominantly by recrystallization, orientated parallel to S4 and surrounded by thin biotite + chloritoid + muscovite bands in ultramylonite. Preferentially elongated quartz grains or polycrystalline aggregates of recrystallized quartz grains are evident, and they possess strongly irregular grain boundaries suggesting grain boundary migration recrystallization and subgrain rotation recrystallization. (f) Sample BL-13 showing that magmatic texture (equigranular K-feldspar and quartz grains) form a triple-junction texture with a weak foliation. Undulatory extinction in quartz and orientated fine biotite and quartz grains indicate a weak syntectonic or post-crystalline deformation. Qtz: quartz, Bi: biotite, Kfs: K-feldspar, Ctd: chloritoid, Ms: muscovite, Hb: hornblende.

3.4.1. Quartz microstructures and c-axis fabrics

This section presents our work on quartz microstructures and CPO fabrics that developed during D4. Preserved microstructures and CPOs reflect the shearing temperature and deformation processes in effect during progressive shear zone evolution. The electron backscatter diffraction (EBSD) analytical procedure and sample descriptions are provided as an electronic supplement (Appendix A).

Detailed EBSD analyses focused on two types of quartz grains in all samples (see Appendix for detailed descriptions; e.g., Fig. 9). The observed *c*-axis distribution (Fig. 10) can be broadly classified into three main fabric types: crossed girdles (similar to Type I crossed girdle fabrics described by Lister and Hobbs (1980)), single girdles with *Y*-maxima, and *X*-maxima.

In general, *c*-axis orientations are concentrated close to the *X*-axis in coarser-grained quartz aggregate sub-regions within mylonite and ultramylonite (e.g., patterns h and j in Fig. 9; regions 2 and 4 of GL-42; regions 1, 2, and 3 of GL-11; all sub-regions of GD-4; all sub-regions of GM-2; regions 1 and 2 of Y05-28; regions 3 and 4

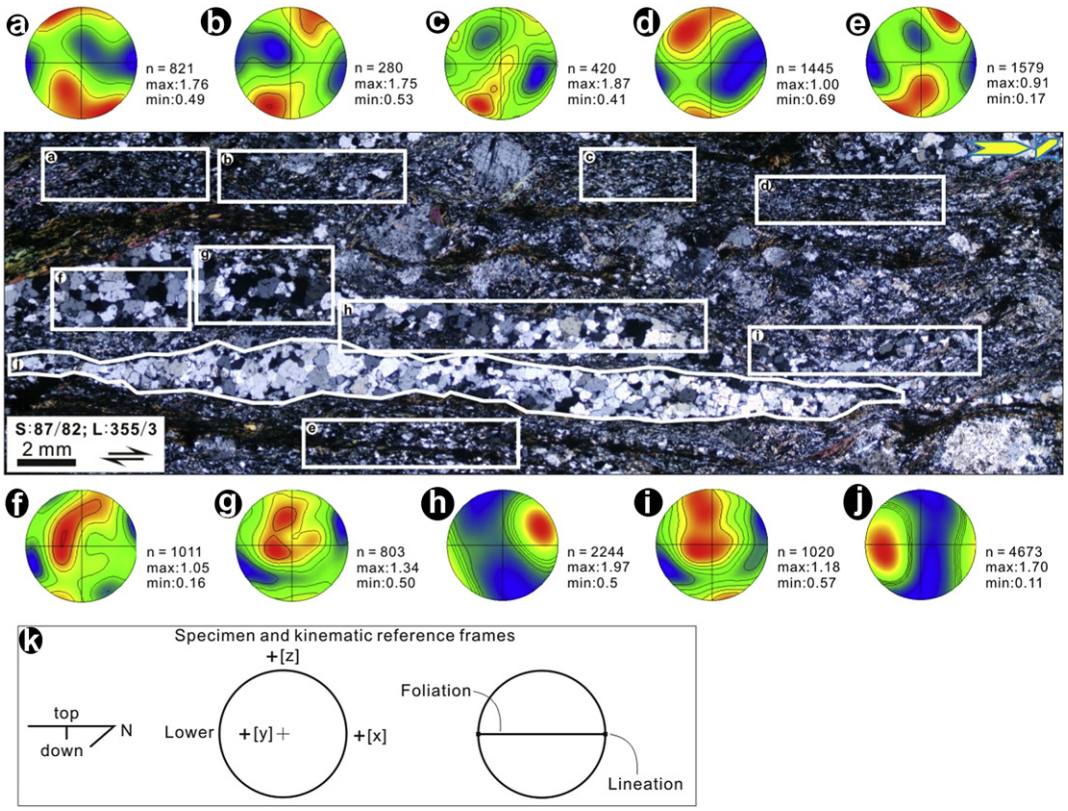

Fig. 9. Photomicrograph of mylonitic granitic gneiss showing quartz microstructure with quartz *c*-axis orientation patterns for various sub-regions in an oriented thin section of sample Y07-22. (a–e) Type B quartz: finer-grained quartz grains and aggregations (grain size: 20–200 μm) in the matrix and their EBSD patterns. (f–j) Type A quartz: coarser-grained quartz (grain size: 50–800 μm) bands and their EBSD patterns. Note: microphotographs show the analyzed sub-regions of quartz bands and their corresponding *c*-axis orientations on stereonet plots (lower hemisphere equal-area projections in which the foliation is horizontal and the lineation is horizontal, E–W). Each band yields a different *c*-axis pattern (this difference has been reported for other mylonites; e.g., Mancktelow and Pennacchioni (2004) and Peternell et al. (2010)). All plots are oriented as indicated in the specimen and kinematic reference frame (k).

of Y05-30 in Fig. 10). The evidence for high-temperature deformation from the CPO pattern is mainly derived from these remnant grains and grain aggregations (Passchier and Trouw, 1996; Toy et al., 2008), which indicate they experienced and/or recorded high-temperature deformation.

Single girdle fabrics with *Y*-axis maximum fabrics are also observed in coarser-grained quartz (type A) bands within mylonite and ultramylonite (e.g., similar patterns f, q, and i in Fig. 9; regions 6 and 7 of GL-42; region 1 of GL-44; region 6 of GM-11 in Fig. 10). These fabrics are always asymmetrical. Most fabrics are rotated clockwise from the *YZ* plane of the samples; however, anticlockwise rotation was also observed (e.g., pattern i in Fig. 9). The *c*-axis maximum close to the *Y*-axis of finite strain represents a slip consistent with on a prism <a> system rather than basal <a> systems (Toy et al., 2008). A quartz texture with a *c*-axis maximum (prism <a> slip system) in the intermediate fabric direction is typical of intermediate–high temperature mylonites (Passchier and Trouw, 1996; Toy et al., 2008). Therefore, *Y*-axis maxima are expected to develop during high strain deformation during amphibolites-facies metamorphism within the lower crust (Toy et al., 2008).

Crossed girdle fabrics occurred mainly in fine-grained regions of recrystallized quartz (e.g., patterns a–e in Fig. 9) within various deformed rock types (all sub-regions of sample GL-8; most sub-regions of GL-13; region 5 of Gl-42; regions 5 and 7 of GM-11 in Fig. 10). Many crossed girdle patterns are asymmetric, while others are slightly symmetric. Asymmetries in Type I crossed girdle fabrics in mylonite may indicate simple shear (Lister and Paterson, 1979; Lister and Hobbs, 1980). Protomylonite and weakly deformed leucogranite samples exhibit two fabric patterns (CPO patterns of GL-8 and GL-13 in Fig. 10). One pattern resembles those expected for type I crossed girdle fabrics (regions 1, 2, and 4 of GL-8; regions 1, 6, and 7 of GL-13 in Fig. 10), while a second pattern forms two small circles around the *Z*-axis of the finite strain ellipsoid (region 3 of GL-8; regions 2–5 of GL-13 in Fig. 10). The *c*-axis maxima in protomylonite and weakly deformed leucogranite are also asymmetrically distributed about the *XY* plane.

Small circle distributions of *c*-axes around the *Z*-axis were reported from rocks in the Tauern Window of the eastern Alps (Wallis and Behrmann, 1996) and in Alpine Fault mylonite (Toy et al., 2008); these were interpreted as deviations from plane strain or as having some degree of non-coaxiality (Wallis and Behrmann, 1996). Our data show that a low degree of non-coaxial strain is more significant in protomylonite and weakly deformed leucogranitic veins within the shear zone than outside of it. We expect the simple shear component in the same sample to be accommodated by thin shear bands and recrystallized grains (Wallis and Behrmann, 1996; Toy et al., 2008). Therefore, the crossed girdle and *Z*-axis maxima patterns observed in protomylonites and weakly deformed leucogranite are interpreted to represent deformation and related strain partitioning under lower-temperature conditions (Mark et al., 2010; Trepmann et al., 2010).

The quartz *c*-axis orientations obtained from EBSD analyses illustrate significant differences between thin sections/samples, and even between sub-regions within the same thin section. Quartz CPOs from ultramylonite and mylonite clearly demonstrate variation between active slip systems, indicating a range of temperature conditions, from high to low (Fig. 10). However, quartz *c*-axis fabrics

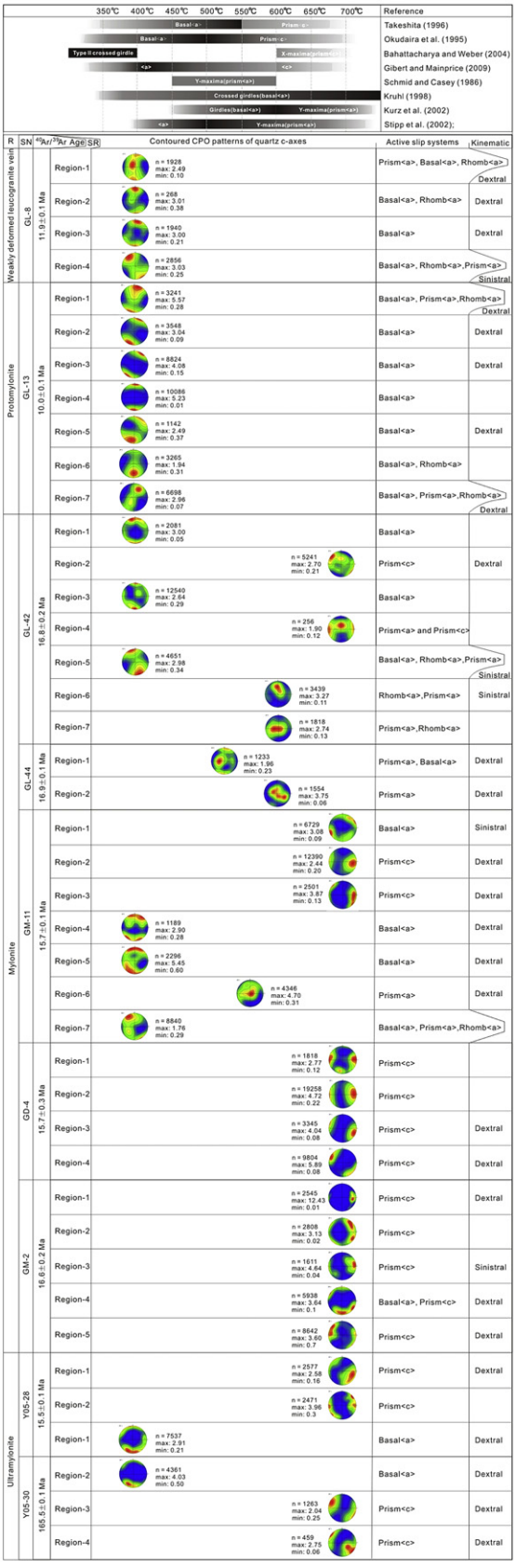

Fig. 10. Summary of the relationships between the estimated temperature, CPO patterns, and transitions between slip systems in quartz (Toy et al., 2008). Quartz CPOs from the Gaoligong shear zone are shown. Columns, from left to right, are rock type, sample No., $^{40}Ar/^{39}Ar$ age, CPO patterns (lower hemisphere equal-area projections showing poles to *c*-axes), active slip system, and corresponding kinematics. All plots are oriented as indicated in the specimen and kinematic reference frame in Fig. 9k.

in protomylonite and weakly deformed leucogranite formed at low temperatures (Fig. 10). In combination with microstructural investigations, we believe this difference most likely indicates that the heterogeneity in quartz *c*-axis preferred orientations is controlled not only by temperature, but by the deformation mechanism (e.g., strain partitioning; Mark et al., 2010; Peternell et al., 2010) and kinematic vorticity (Lister and Hobbs, 1980; Wallis and Behrmann, 1996). Differences between quartz CPOs in the same thin section are evidence for micro-scale strain partitioning. The fabric analysis clearly demonstrates that conflicting shear senses occur within the same thin section (e.g., Fig. 9), supporting the concept of strain partitioning in a setting with a low degree of bulk vorticity (Fossen and Tikoff, 1993; Wallis and Behrmann, 1996; Jones et al., 1997, 2004; Halfpenny et al., 2006). The observed clockwise rotation of fabric elements in *c*-axis plots indicates a dextral-dominated shear sense (Fig. 10), consistent with the overall displacement sense of the zone. The observed *c*-axis maxima patterns are mostly distributed away from the *X*-axis (clockwise). Hence, the clockwise rotation of these fabric elements is reliably used to infer the dextral shear sense (Passchier and Trouw, 1996).

4. Isotope geochronology: $^{40}Ar/^{39}Ar$ dating of mica

Constraining the absolute timing and duration of ductile shear deformation is critical for establishing regional correlations between tectonic deformation events and P–T–t paths (Dunlap, 1997; Rolland et al., 2009). Shear zone deformation can be directly dated using syn-kinematic intrusions; metamorphic minerals that formed/cooled during shearing; or pre- and post-kinematic intrusions (Searle, 2006). The $^{40}Ar/^{39}Ar$ method permits the deciphering of the thermotectonic history of metamorphic minerals, and is particularly appropriate for cases where overprinting of metamorphic episodes has occurred (McDougall and Harrison, 1999). Sample descriptions and the $^{40}Ar/^{39}Ar$ analytical methodology employed are provided as an electronic supplement (Appendix B).

4.1. Analytical results

Nine biotite analyses yielded identical weighted mean plateau ages (WMPA), inverse isochron ages (IIA), and normal isochron ages (NIA) within analytical error (1σ). The values of NIA and total fusion age (TFA) are commonly younger than those of the WMPA. The analyses cluster into two groups (Fig. 11; Table 2). Group I includes seven analyses from seven representative mylonite and ultramylonite samples. Biotite occurs as small grains that define the stretching lineation upon shear planes. Biotite separates from six samples yielded well-defined plateau ages during intermediate–high-temperature heating steps (Fig. 11). The corresponding plateau ages are 16.8 ± 0.2 Ma (GL-42), 16.9 ± 0.1 Ma (GL-44), 15.7 ± 0.1 Ma (GM-11), 16.6 ± 0.2 Ma (GM-2), 15.5 ± 0.1 Ma (Y05-28), and 16.3 ± 0.1 Ma (Y05-30). These ages are defined by more than 90% (65% for GM-2) of total ^{39}Ar release, and their initial $^{40}Ar/^{36}Ar$ ratios range from 288 to 296, consistent with the present atmospheric $^{40}Ar/^{36}Ar$ ratio of 295.5. Biotite from sample GD-4 yielded variable apparent ages during intermediate–high-temperature heating steps but well-defined plateau ages during low-temperature steps. The plateau age of 15.7 ± 0.3 Ma is well-defined, with over 30% of ^{39}Ar gas released. Samples yielded WMPAs, IIAs, and NIAs ranging from 15.5 to 16.9 Ma. Their WMPAs are generally, within an acceptable error, identical to calculated inverse isochron ages. The age difference between samples, corresponding to different sample sites within the shear zone, does not exceed 2 Ma. These results indicate that progressive shear

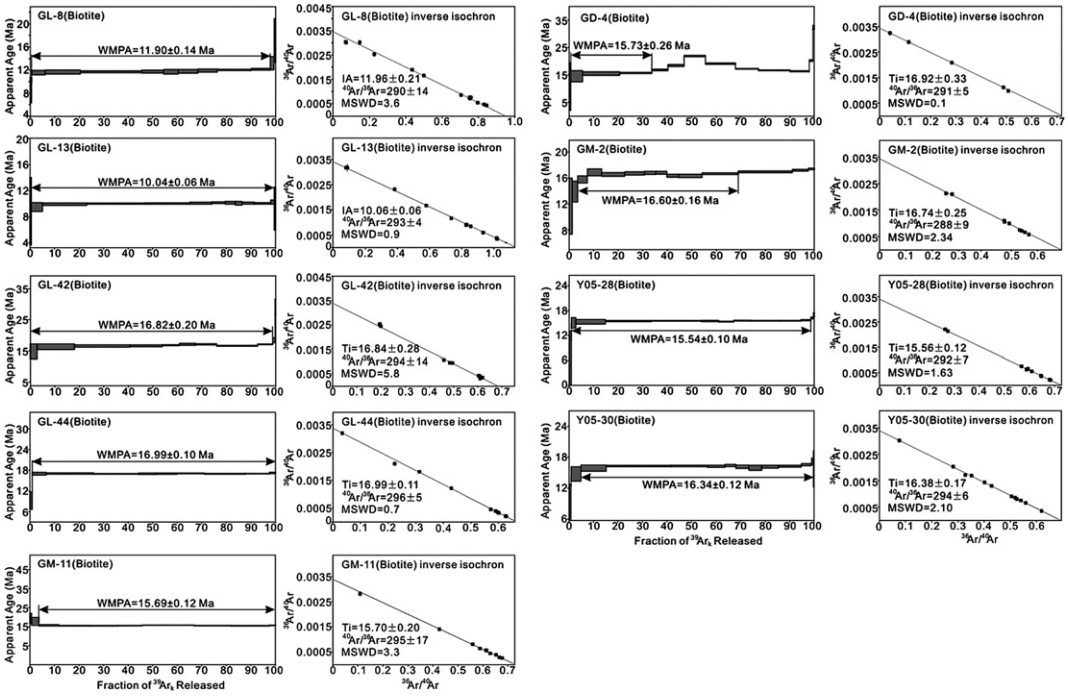

Fig. 11. Age spectra and inverse isochron plots for biotite samples from the Gaoligong shear zone.

deformation characterizes D4, rather than distinct stages (Rolland et al., 2009).

Group II consists of two analyses from samples of a weakly deformed leucogranitic vein and protomylonite. Their plateau ages range from 11.9 to 10.1 Ma, which is the same as the ranges obtained for IIA and NIA (10.1–11.9 Ma) within acceptable error (Fig. 11).

4.2. Interpretations

The samples from Group I are from mylonite and ultramylonite in the shear zone, where primary magmatic biotite grains were strongly deformed, resulting in small fragments clustering in strips (Fig. 8b, c). The dated biotites are aligned along the foliation in mylonitic rocks, recrystallized during the D4 deformation event. Tails and strain shadows on K-feldspar and quartz porphyroclasts are formed of quartz + biotite + muscovite ± chlorite (Fig. 8a, b, c, e), which are low-grade greenschist facies minerals. Quartz shows a strong shape-preferred orientation, undulose extinction, grain boundary migration recrystallization (GBMR), and subgrain rotation recrystallization (SR), indicating deformation temperatures of at least ~500 °C (Fig. 8a, b, e; Passchier and Trouw, 1996; Langille et al., 2010). Feldspar porphyroclasts show undulatory extinction, indicating temperatures above 450 °C (Fig. 8b, c; Langille et al., 2010). The CPO patterns of quartz <c> indicate intermediate–high deformation temperatures ranging from 400 to 650 °C or higher (Fig. 10). Thus, the K–Ar isotope system of primary biotite was completely reset during ductile shearing (Dunlap, 1997; Searle, 2006; Lin et al., 2009). The aforementioned $^{40}Ar/^{39}Ar$ plateau ages of 15.5–16.9 Ma represent the age of cooling through appropriate argon closure temperatures in biotite (300–350 °C; Dodson, 1973), providing a minimum age of 16.9 Ma for the onset of shearing.

Group II biotite fragments were sampled from the weakly deformed leucogranitic veins and the protomylonite. Field observations show that the analyzed veins are synchronous with shearing and related melting. The two analyses give WMPAs ranging from 11.9 to 10.0 Ma, similar to the $^{40}Ar/^{39}Ar$ ages from leucogranites along the Gaoligong shear zone and gneiss dated by Lin et al. (2009). Quartz in the protomylonitic rocks exhibits undulatory extinction, but lacks microfractures (Fig. 8f), indicating temperatures of at least ~350 °C (Passchier and Trouw, 1996; Langille et al., 2010). Based on quartz CPO patterns from samples GL-8 and GL-13, quartz *c*-axis fabrics are dominated by basal <a> gliding patterns, which also suggest deformation

Table 2
Summary of $^{40}Ar/^{39}Ar$ geochronological data and mineral assemblage features for each sample.

Sample	Rock type	Mineral assemblage	AM	*J*-value	WMPA Ma	IIA Ma	NIA Ma	TFA Ma	MSWD
GL-8	WDG	Kfs + Pl + Qtz + Bi + Ms + Hbl	Bt	0.006322	11.90 ± 0.14	11.96 ± 0.21	11.95 ± 0.21	11.84 ± 0.11	3.45
GL-13	G-PMy	Kfs + Pl + Qtz + Bi + Ms + Hbl	Bt	0.00633	10.04 ± 0.06	10.06 ± 0.07	10.06 ± 0.07	9.98 ± 0.09	0.93
GL-42	G-My	Kfs + Pl + Qtz + Bi + Ms + Hbl	Bt	0.006389	16.82 ± 0.20	16.84 ± 0.28	16.82 ± 0.28	16.44 ± 0.21	5.11
GL-44	G-My	Qtz + Pl + Kfs + Bi + Chl	Bt	0.006310	16.99 ± 0.10	16.99 ± 0.11	16.99 ± 0.11	16.92 ± 0.12	0.63
GM-11	G-My	Kfs + Pl + Qtz + Bi + Ms + Chl	Bt	0.006376	15.69 ± 0.12	15.70 ± 0.20	15.69 ± 0.20	15.77 ± 0.12	2.88
GD-4	G-My	Pl + Bi + Ms + Hbl + Qtz	Bt	0.006383	15.73 ± 0.26	15.92 ± 0.33	15.93 ± 0.33	17.33 ± 0.19	1.06
GM-2	G-My	Qtz + Pl + Kfs + Bi	Bt	0.006361	16.60 ± 0.16	16.74 ± 0.25	16.74 ± 0.25	16.61 ± 0.13	2.63
Y05-28	G-UMy	Kfs + Pl + Qtz + Bi + Chl	Bt	0.006272	15.54 ± 0.10	15.56 ± 0.12	15.56 ± 0.12	15.15 ± 0.10	1.54
Y05-30	G-UMy	Kfs + Pl + Qtz + Bi + Ms + Chl	Bt	0.006298	16.34 ± 0.12	16.38 ± 0.17	16.38 ± 0.17	16.14 ± 0.14	1.97

WMPA-weighted mean plateau age; IIA-inverse isochron age; NIA-normal isochron age; TFA-total fusion age; AM-analyzed mineral; Chl-Chlorite; Kfs-Kfeldspar; Pl-Plagioclase; Qtz-Quartz; Bi-Biotite; Ms-Muscovite; Hbl-Hornblende; G-granitic; UMy-ultramylonite; My-mylonite; PMy-protomylonite; WDG-weakly deformed leucogranitic vein.

temperatures of ~400 °C or <400 °C (Fig. 10). The K–Ar isotope system of biotite may be partially or completely reset during shear deformation (Searle, 2006; Lin et al., 2009). The $^{40}Ar/^{39}Ar$ plateau ages of 11.9 to 10.0 Ma likely represent cooling ages through appropriate argon closure temperatures in biotite (300–350 °C; Dodson, 1973). These ages also provide likely ages for continued ductile shearing within the zone.

The $^{40}Ar/^{39}Ar$ analyses of variably deformed granitic rocks along the shear zone indicate that mylonites with older age dates experienced deformation at intermediate–high temperatures, while protomylonite and veins with younger age dates experienced deformation at low–intermediate temperatures (Fig. 12). In summary, detailed $^{40}Ar/^{39}Ar$ analyses indicate that D4 ductile shearing along the Gaoligong zone occurred primarily from ~16.9–15.5 Ma, and continued at 11.9 Ma and 10.0 Ma. Our data are roughly in agreement with $^{40}Ar/^{39}Ar$ results reported by Lin et al. (2009) and are younger than the data published by Wang et al. (2006).

5. Discussion

5.1. Structural correlation and history

The earliest structures (D1) observed in outcrops are relics of tight to isoclinal upright F1 folds and penetrative S1 foliations. Microstructural observations from oriented XZ surfaces show crenulated S1 as a sub-vertical foliation. Evidence for early medium- or high-pressure metamorphism, and the temperature history of the D1 domain of the Gaoligong Group, have previously been reported by Song et al. (2010) and Zhong, 2000 (Fig. 2). These studies suggest that D1 structures and metamorphism are related to crustal thickening in the Gaoligong region (seeing also Yeh et al., 2008; Figs. 5a and 6a; Song et al., 2010) (Fig. 13a). A compilation of published radiometric isotope age data for the zone shows that high-temperature/low-pressure metamorphism probably continued to the onset of the Indosinian orogeny (Zhong, 2000).

Based on studies of sedimentary and mafic–ultramafic rocks, one important compressional event, a major orogeny, occurred in the Late Permian (Carter et al., 2001) or Early Triassic (Ji et al., 2009). The Sibumasu block converged and collided with Indochina. The Malaya block moved along the Uttaradit–Nan and Bentong–Raub suture during the Late Permian. Farther west, the northern Palaeo-Tethys closed with widespread Late Triassic orogenic folding (Carter et al., 2001; Yeh et al., 2008). In western Yunnan, the Baoshan and Gengma blocks, corresponding to the Sibumasu block, converged toward the Tengchong block due to subduction and closure of the Palaeo-Tethys ocean basin during the Late Permian (Fang, 1994; Zhong, 2000). Given that Gangdese belt rock units show some similar SHRIMP U–Pb and $^{40}Ar/^{39}Ar$ ages (245 Ma; Ji et al., 2009), Ji et al. (2009) suggested that Early Triassic subduction caused regional metamorphism and magmatism, interpreting this event to mark the onset of the Indosinian orogeny.

On the basis of the similar age span for regional metamorphism and the same NW–SE trend of D1 structures along the Biluoxueshan–Chongshan belt (Zhang et al., 2010), we interpret that D1 structures are the result of the amalgamation of the Baoshan and Tengchong micro-blocks in the Late Permian–Early Triassic Indosinian orogeny (Fig. 13a). D1 events are constrained to the Early Triassic to Late Cretaceous, resulting from progressive shortening during collision, which caused the crustal thickening and metamorphism (M1) of Paleozoic rocks (Fig. 2). On the basis of observed F1 features in outcrops, we interpret the D1 strain field as a response to the NE–SW-directed contraction. Goscombe and Trouw (1999) point out that refolding of early foliations and associated shear sense indicators is often not fully considered and may potentially lead to incorrect tectonic interpretations (Yeh et al., 2008). Combined with the regional model for Tertiary rotation (Wang and Burchfiel, 1997), we limit our interpretations of the D1 strain field as a response to the NE–SW directed contraction, similar to the Day Nui Con Voi metamorphic complex (Yeh et al., 2008).

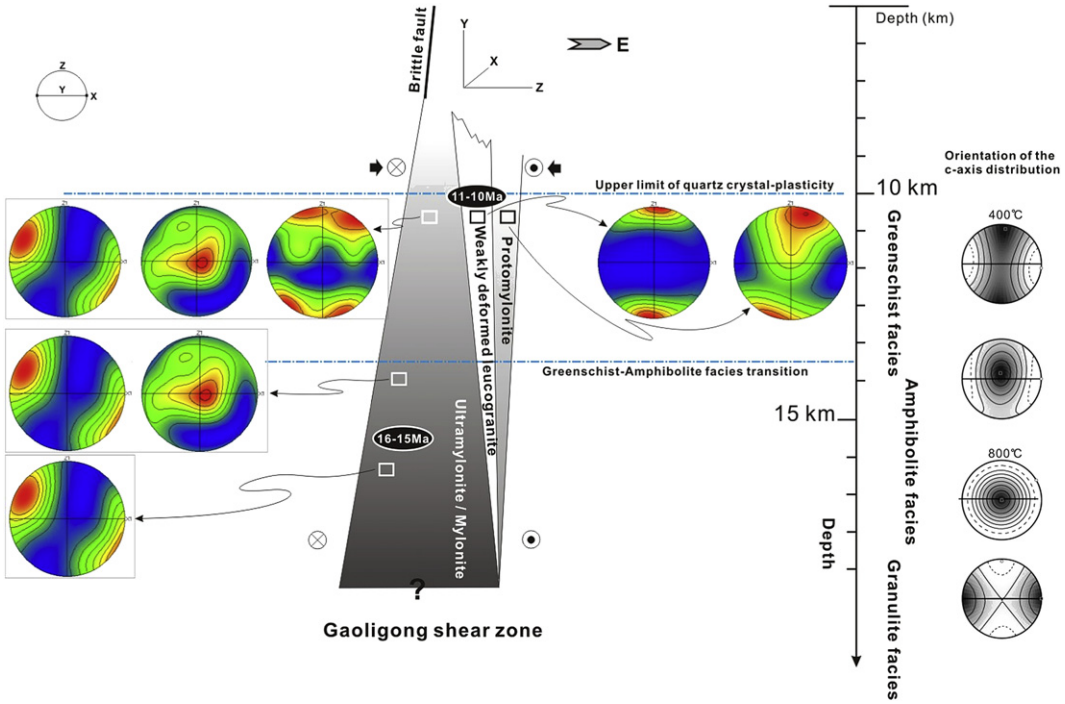

Fig. 12. Cartoon showing the progressive development/preservation of quartz CPOs in various tectonites during shearing and exhumation since ca. 16 Ma in the Gaoligong mylonite zone. The change in orientation of the quartz *c*-axis distribution with depth is from Toy et al. (2008), Gibert and Mainprice (2009) and Stipp and Kunze (2008). The upper limit of quartz crystal-plasticity is estimated by Hirth and Tullis (1992). Numbers in ellipses represent the $^{40}Ar/^{39}Ar$ mica age ranges from this study.

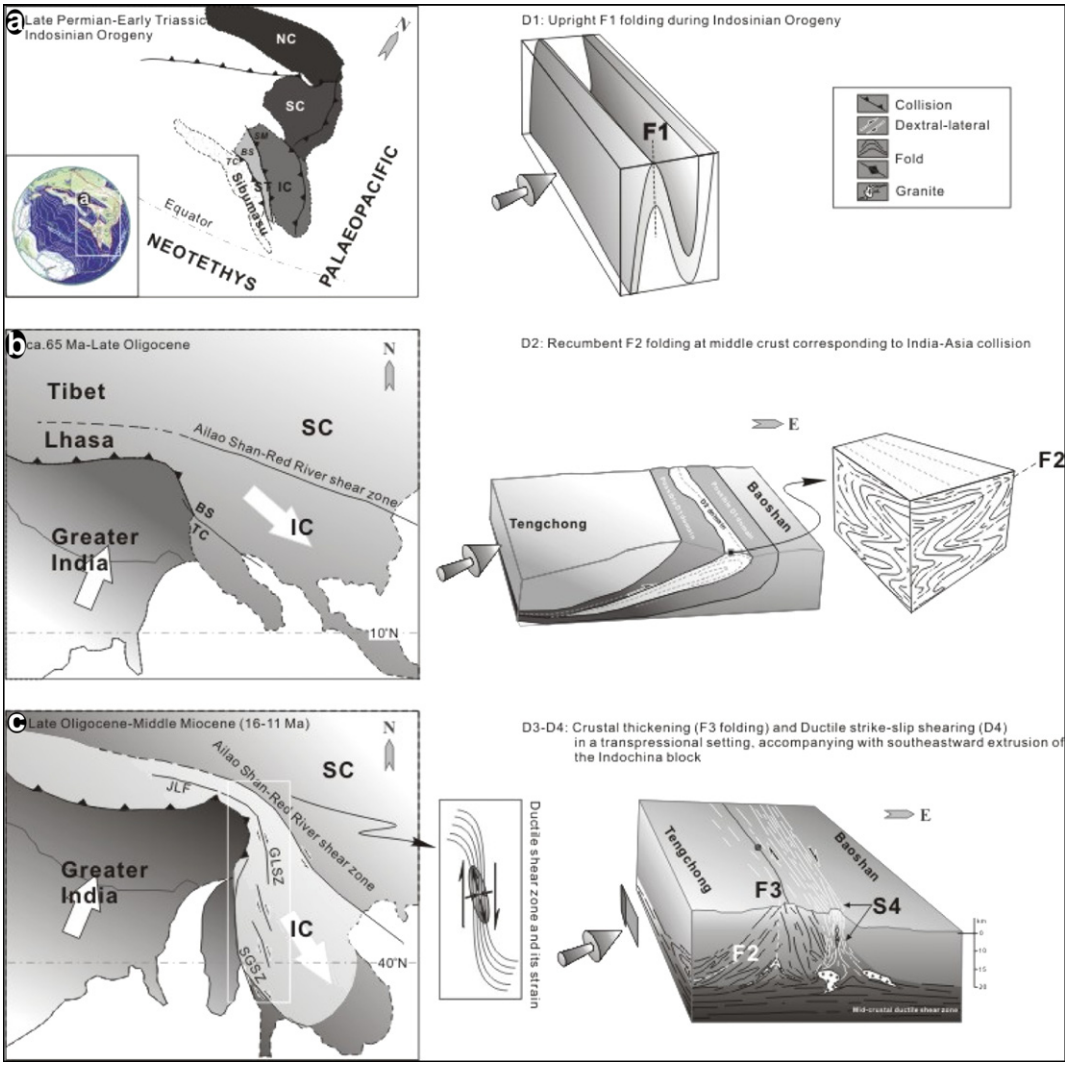

Fig. 13. Sequential diagrams showing four major deformation stages responsible for the pre-Miocene structures of the Gaoligong zone (modified from Carter et al. (2001), Jolivet et al. (2001), Metcalfe (2002), Ferrari et al. (2008), Yeh et al. (2008), Lin et al. (2009), Searle et al. (2010)). NC: North China; SC: South China; IC: Indochina; ST: Shan–Thai; SM: Simao; BS: Baoshan; TC: Tengchong; JLF: Jiali fault; GLSZ: Gaoligong shear zone; SGSZ: Sagaing shear zone. (a) Upright F1 fold suggests an early period of contractional folding and high-grade metamorphism in metasediments of Paleozoic rocks due to the Indosinian orogen or an earlier event (geodynamic reconstruction during the Indosinian orogen is from Metcalfe (2002), Ferrari et al. (2008)). (b) Continued collision results in buttressing and lateral escape that likely occurred at mid-crust levels since ca. 65 Ma (geodynamic reconstruction in this stage is modified from Yeh et al. (2008)). The lateral escape or flow is manifested by regional recumbent F2 folding and sub-horizontal N–S mineral lineations, which indicate horizontal or sub-horizontal shearing (Royden et al., 1997; Clark and Royden, 2000). (c) Maximum thickening and a regional change to dextral transpression. The regional dome formed during the late Oligocene to middle Miocene (geodynamic reconstruction in this stage is modified from Socquet and Pubellier (2005), Yeh et al. (2008)). In this stage, the Gaoligong shear zone (D4 deformation) developed and localized into a narrow ductile zone along the east limb of a regional F3 fold. Enhanced partial melting and intrusion of leucogranite into/along S3 suggests that D4 deformation occurred at high temperatures. The Gaoligong shear zone is flattened and rooted in the middle crust at depths of ~15–20 km (Bai and Meju, 2003; Li et al., 2008; Huang et al., 2009; Wang et al., 2008; Zhang and Wang, 2009; and CPO patterns in this study). The cooling ages from $^{40}Ar/^{39}Ar$ geochronology suggest the onset of D4 deformation was earlier than ~16 Ma in the middle crust, and continued to ~11 Ma in the middle–upper crust.

D2 is the major deformation and metamorphic event to affect the study area, generating tight to isoclinal F2 folds with a penetrative S2 foliation. F2 folds with a sub-horizontal axial planar S2 foliation suggest vertical shortening with top to the east, and west-directed shearing in the Pianma and Tengchong sections, respectively, which rotated F1 folds into recumbent orientations. Sillimanite grains aligned parallel to S1 and S2 represent metamorphic mineral growth during D2/M2 (Fig. 2; Ding, 1991). Ji et al. (2009) reported Pb/Th/U zircon ages of 255–24 Ma for the Gaoligong gneiss. By compiling $^{40}Ar/^{39}Ar$ ages of biotite and hornblende from mylonite (Ji et al., 2000; Wang et al., 2006; Lin et al., 2009), $^{40}Ar/^{39}Ar$ ages for whole rock of mafic dykes (Xu et al., 2008), U–Pb zircon ages from leucogranite within the zone (Song et al., 2010), and the closure temperatures for the various minerals (Wang et al., 2006; Lin et al., 2009; Song et al., 2010; Xu et al., 2008), it is estimated that metamorphic conditions throughout the entire Gaoligong gneiss zone remained above 500 °C until 24 Ma; rapid cooling did not occur prior to 24 Ma (Fig. 13b). With exclusively top to the WNW and ESE-directed shearing, and considering the flat-lying sillimanite mineral lineation in the gneiss, we infer that F2 folds resulted from simple shear during mid-crustal flow (Fig. 13b). Various shear senses in the Pianma and Tengchong blocks support this interpretation. Similar structures were also recognized within the Dai Nui Con Voi metamorphic zone, in the southern segment of the Ailao Shan gneiss zone, by Jolivet et al. (2001) and Yeh et al. (2008). The exhumation history of the Dai Nui Con Voi metamorphic rocks shows that they were first deformed at depth along a horizontal shear zone and later reworked by steeper shear deformation (Jolivet et al., 2001).

The younger D3 ductile deformation that resulted in the gneiss antiform was identified along the Gaoligong zone. D3 deformation formed a sub-vertical S3 foliation with a shallowly plunging mineral stretching lineation that strikes NNW–SSE. Song et al. (2010) interpreted this event as a regional medium- to high-pressure granulite facies metamorphic event that occurred in the Gaoligong Group as a result of crustal thickening prior to ca. 22 Ma (Fig. 13c).

In contrast to the D1–D3 ductile folding events, D4 deformation produced semi-ductile to ductile strike-slip shearing fabrics that cross-cut earlier fabrics in outcrop. D4 features have been inferred as the result of exhumation following a period of crustal thickening (Fig. 13c). Jolivet et al. (2001) and Yeh et al. (2008) concluded that pre-existing sub-horizontal mid-crustal gneisses were uplifted in a late transpressional crustal corridor (Figs. 12, 13b, c). Based on CPO patterns preserved in the various mylonitic gneisses, we suggest that the Gaoligong gneiss was subjected to shearing and uplift in a ductile transpressive regime (Fig. 12). As shown in Fig. 12, ideal CPO plots represent possible quartz CPO patterns developed during exhumation from deeper crustal levels. In the later stages of exhumation, or at a certain shallow level, protomylonites and weakly deformed leucogranites formed a strong preferred orientation fabric of *Z*-maxima, similar to one of the fabrics developed in mylonites and ultramylonites. However, ultramylonite and mylonite exhumed through the granulite to amphibolite facies transition would only contain the strong preferred orientation pattern of *X*-maxima (Gibert and Mainprice, 2009). The amphibolite to greenschist facies transition might only contain a strong preferred orientation pattern of *Y*-maxima (Toy et al., 2008; Gibert and Mainprice, 2009). Obviously, the patterns for *X*- and *Y*-maxima are not easily destroyed during subsequent low-temperature deformation (Toy et al., 2008). In this model, the starting CPO is shown as the *X*-maximum pattern suggested by Gibert and Mainprice (2009). The early-stage strong CPOs were preserved in mylonites and ultramylonites. Protomylonite and weakly deformed leucogranite do not preserve indicators of early-stage high-temperature fabrics, unlike the mylonites and ultramylonites (Fig. 12).

More than one type of CPO pattern is preserved in an individual sample. Therefore, we interpret the preservation of the high-temperature fabric in the mylonites and ultramylonites as a result of their intense *Y*- and/or *X*-maxima, indicating that few grains were suitably oriented for basal <a> slip. Consequently, the first slip system to be activated during shear remains the prism <a> system (Toy et al., 2008). At shallow levels, fabric development under the previous conditions would result in crossed girdle patterns and/or distribution around the *Z*-maximum (Heilbronner and Tullis, 2006; Toy et al., 2008). In combination with our $^{40}Ar/^{39}Ar$ data collected from various tectonites, the observed fabric changes and transitions may represent different degrees of preservation of high-temperature CPOs during ductile deformation. Mylonite and ultramylonite possess various CPOs, with *c*-axes preferentially clustering near the *X*-, *Y*-, and *Z*-axes. Since ultramylonite and mylonite that experienced the complete evolution of ductile shearing and exhumation since ~16 Ma preserve various fabrics, it is reasonable to assume that some of the fabrics were inherited from the "starting material" (Fig. 12; Stipp and Kunze, 2008). Protomylonite and weakly deformed leucogranite possess preferential *c*-axis orientations near the *Z*-axis and have younger $^{40}Ar/^{39}Ar$ ages (Figs. 10 and 12). Since the protomylonite and leucogranite veins preserve lower-temperature ductile fabrics and were not strongly affected by the Gaoligong shear zone, we speculate that at least some of the fabrics formed at shallow crustal levels during the later stage of shearing (11–10 Ma; Fig. 12).

During the D3 and D4 events, the zone underwent a transition from crustal thickening to shearing and exhumation accompanied by widespread decompression metamorphism (M3 in Fig. 2 of Ding, 1991, Fig. 12), which is represented by the growth of orthopyroxene and plagioclase in the mafic granulites (Song et al., 2010). The occurrence of medium- to high-pressure granulite facies metamorphic rocks in the Gaoligong metamorphic zone (Song et al., 2010) and in the Baoshan and Tengchong blocks (BGMRYP, 1990; Ji et al., 2000) suggests a regional high-P–T metamorphic event prior to the Miocene (ca. 17 Ma), and these rocks not associated with, or spatially restricted to, the narrow ductile shear zone (Song et al., 2010; this study). Microstructural analyses and mineral assemblages indicate that dextral strike-slip mylonitization was a later greenschist-facies metamorphic event, and overprinted earlier regionally occurring high-grade metamorphic rocks. Finally, the zone was exhumed to shallow crustal levels where all lithologies experienced cooling and retrograde metamorphism.

We suggest that rocks within the Gaoligong shear zone were not formed as a result of shear heating during strike-slip faulting, but are basement rocks (possibly Permian–Triassic in age) that were uplifted and experienced high-temperature overprinting in the Miocene (D3 crustal thickening and D4 strike-slip shearing) that resulted in localized partial melting to form leucogranite veins. The marbles outside of the Gaoligong shear zone in the Tengchong area show that regional high-grade metamorphism was not restricted to the shear zone (Song et al., 2010). High-grade marbles in Baoshan, east of the Gaoligong mountain chain, also preserve evidence of regional metamorphism outside of the shear zone (BGMRYP, 1990; Zhong, 2000).

The four stages of deformation preserved in the zone record progressive tectonism that involved initial crustal thickening, horizontal shearing, later crustal thickening, ductile strike-slip shearing, and uplift/exhumation. This is consistent with intracontinental deformation that was initiated during the collision of the Baoshan and Tengchong blocks during the Indosinian orogeny.

5.2. Tectonic interpretation

Tapponnier et al. (1982) originally proposed the indentation–extrusion model as a tectonic mechanism to explain large-scale strike-slip fault systems in Asia. Sub-vertical foliations/cleavages with sub-horizontal stretching lineations and sub-vertical folds are generally associated with strike-slip tectonics. However, our field data from the Gaoligong zone show that sub-horizontal shearing also played an important role in the region's metamorphic and structural evolution. The presence of a sub-horizontal foliation within other zones in the Indochina block, such as that within the Day Nui Con Voi metamorphic complex (DNCV), has long been known (e.g., Jolivet et al., 2001; Leloup et al., 2001; Tapponnier et al., 2001). Leloup et al. (2001) reported this to be the main difference between the DNCV in Vietnam and other metamorphic zones of the Ailao Shan–Red River shear zone, and proposed that the sub-horizontal nature of the foliation resulted from vertical flattening during left-lateral transtensional movement along the zone. However, Jolivet et al. (2001) and Searle (2006) suggested that strike-slip faults are not necessarily deeply rooted, and thus may not cut through the entire lithosphere. The DNCV deformed at depth along a horizontal shear zone prior to exhumation along steep shear zones, which is further supported by microstructural and fabric analysis (Yeh et al., 2008). Based on our structural investigations and the ideas of Jolivet et al. (2001) and Yeh et al. (2008), the exhumation history of the zone that was first deformed at depth, most likely occurred along a horizontal shear zone and was later reworked by transpressional deformation. These investigations suggest that strike-slip shearing along the Gaoligong

shear zone did not affect the deep crust. Instead, shearing was restricted to the middle and upper crust above a lower-crustal domain where horizontal shear zones predominate.

Figs. 12 and 13c show the possible structural geometry at depth during shear zone activity. In this scenario the upper crust is cut by a right-lateral fault system. The fault roots reach the brittle–ductile transition zone where ductile shearing occurs under greenschist facies conditions. The steep shear zone, in turn, branches into a horizontal shear zone that separates the upper and middle crust from the lower crust. High-temperature deformation may have been active along the horizontal shear zone and below it (Jolivet et al., 2001; Li et al., 2008). Similar regional metamorphic conditions and fabrics have also been investigated outside of the Ailao Shan–Red River shear zone, as in the Truong Son belt (Lepvrier et al., 1997) and the Song Chay dome (Jolivet et al., 2001). Geochronologic data from monazite inclusions in garnet porphyroblasts indicated that high-temperature rocks can be maintained at mid-crustal levels for about 10 My (Gilley et al., 2003). This suggests that D2 was a long-lasting event, and that the dominant heat source for amphibolite facies metamorphism in the mid-crust was radioactive self-heating and rheological weakening of thickened crust (Jolivet et al., 2001; Aoya and Wallis, 2003; Yeh et al., 2008).

6. Conclusions

The Gaoligong metamorphic zone in western Yunnan underwent three stages of folding followed by ductile shearing during the Permian–Tertiary. Upright D1 folds record the early collision of the Indosinian orogeny, when the Tengchong and Baoshan blocks collided. D1 resulted in crustal shortening and thickening. D2 subsequently overprinted D1 and produced recumbent folds that formed along a horizontal shear zone at mid-crustal levels. D3 produced dome structures and was responsible for a second period of crustal thickening in the region. Rapid cooling occurred at ~16 Ma along the zone, and the dextral transpressional D3–D4 event exhumed the Gaoligong zone. The four stages of deformation in the zone record tectonic processes characterized by an initial period of crustal thickening and horizontal shearing in the middle crust, followed by subsequent transpressional deformation and exhumation. The related metamorphic rocks are exhumed along but not restricted to the Gaoligong shear zone.

Acknowledgments

This work was supported by the National Natural Science Foundation of China for Young Scientists (Grant numbers 40802050 and 40872149) and the China Postdoctoral Science Foundation (Grant number 20070420065). The authors thank Jacques Charvet and Zheng Yadong for critical and constructive comments, and suggestions that improved the original version of the manuscript. Wang Erqi, Xiao Wenjiao, Ding Lin, Song Shuguang, and Liu Junlai are gratefully acknowledged for their suggestions on an early version of the manuscript. We thank Dr. A. Alexander G. Webb for discussions and for help refining this manuscript. Qu Junfeng and Guo Lei are thanked for assistance with fieldwork. We are grateful to Prof. David Mainprice, Prof. Steven Reddy, Prof. Zhao Zhongyan, and Dr. Luiz F.G. Morales for helpful comments and discussions on EBSD and quartz CPOs. We gratefully acknowledge the technical help of Dr. Lai Qizhou. Constructive reviews by Prof. Joao Hippertt and Simon R. Wallis improved the manuscript.

Appendix. Supplementary material

Supplementary material associated with this article can be found, in the online version, at doi:10.1016/j.jsg.2012.02.007.

References

Akciz, S., Burchfiel, B.C., Crowley, J.L., Chen, L., Yin, J., 2003. Gaoligong and Chong Shan Shear Zones, Yunnan and accommodation of the northward movement of India relative to Indochina during mid-Cenozoic time. In: AGU 2003 Fall Meeting, San Francisco, CA, USA.

Aoya, M., Wallis, S.R., 2003. Role of nappe boundaries in subduction-related regional deformation: spatial variation of meso- and microstructures in the Seba eclogite unit, the Sambagawa belt, SW Japan. Journal of Structural Geology 25, 1097–1106.

Bai, D.H., Meju, M.A., 2003. Deep structure of the Longling-Ruili fault underneath Ruili basin near the eastern Himalayan syntaxis: insights from magnetotelluric imaging. Tectonophysics 364, 135–146.

BGMRXZR (Bureau of Geology and Mineral Resources of Xizang Autonomous Region), 1993. Regional Geology of Xizang (Tibet) with 1/1,500,000 Geological Map. Geological Publishing House, Beijing (In Chinese with English abstract).

BGMRYP (Bureau of Geology and Mineral Resources of Yunnan Province), 1990. Regional Geology of Yunnan Province. Geological Publishing House, Beijing (In Chinese with English abstract).

Carter, A., Roques, D., Bristow, C., Kinny, P., 2001. Understanding Mesozoic accretion in southeast Asia: significance of Triassic thermotectonism (Indosinian orogeny) in Vietnam. Geology 29, 211–214.

Chen, F.K., Li, Q.L., Wang, X.L., Li, X.H., 2006. Zircon age and Sr-Nd-Hf isotopic composition of migmatite in the eastern Tengchong block, western Yunnan. Acta Petrologica Sinica 22, 439–448.

Chung, S.L., Chu, M.F., Ji, J.Q., O'Reilly, S.Y., Pearson, N.J., Liu, D.Y., Lee, T.Y., Lo, C.H., 2009. The nature and timing of crustal thickening in Southern Tibet: geochemical and zircon Hf isotopic constraints from postcollisional adakites. Tectonophysics 477, 36–48.

Chung, S.L., Chu, M.F., Zhang, Y.Q., Xie, Y.W., Lo, C.H., Lee, T.Y., Lan, C.Y., Li, X.H., Zhang, Q., Wang, Y.Z., 2005. Tibetan tectonic evolution inferred from spatial and temporal variations in post-collisional magmatism. Earth-Science Reviews 68, 173–196.

Clark, M.K., Royden, L.H., 2000. Topographic ooze: building the eastern margin of Tibet by lower crustal flow. Geology 28, 703–706.

Ding, L., 1991. The characteristics of deformation and tectonic implications in south Gaoligong, western Yunnan, China. Dissertation for the Master Degree. Beijing: Institute of Geology, Chinese Academy of Science. pp. 1–88.

Dodson, M.H., 1973. Closure temperature in cooling geochronological and petrological systems. Contributions to Mineralogy and Petrology 40, 259–274.

Dunlap, W.J., 1997. Neocrystallization or cooling? $^{40}Ar/^{39}Ar$ ages of white micas from low-grade mylonites. Chemical Geology 143, 181–203.

Fang, Z., 1994. Biogeographic constraints on the rift-drift-accretion history of the Sibumasu block. In: Gondwana Dispersion and Asian Accretion. Journal of Southeastern Asian Earth Science, 9, pp. 375–385.

Ferrari, O.M., Hochard, C., Stampfli, G.M., 2008. An alternative plate tectonic model for the Palaeozoic-early Mesozoic Palaeotethyan evolution of southeast Asia (Northern Thailand-Burma). Tectonophysics 451, 346–365.

Fossen, H., Tikoff, B., 1993. The deformation matrix for simultaneous simple shearing, pure shearing and volume change, and its application to transpression-transtension tectonics. Journal of Structural Geology 15, 413–422.

Gibert, B., Mainprice, D., 2009. Effect of crystal preferred orientations on the thermal diffusiveity of quartz polycrystalline aggregates at high temperature. Tectonophysics 465, 150–163.

Gilley, L., Harrison, T., Leloup, P.H., Ryerson, F., Lovera, O., Wang, J.H., 2003. Direct dating of left-lateral deformation along the Red River shear zone, China and Vietnam. Journal of Geophysical Research 108, 14–21.

Goscombe, B., Trouw, R.A.J., 1999. The geometry of folded tectonic shear sense indicators. Journal of Structural Geology 21, 123–127.

Halfpenny, A., Prior, D.J., Wheeler, J., 2006. Analysis of dynamic recrystallization and nucleation in a quartzite mylonite. Tectonophysics 427, 3–14.

Heilbronner, R., Tullis, J., 2006. Evolution of c axis pole figures and grain size during dynamic recrystallization: results from experimentally sheared quartzite. Journal of Geophysical Research 111 (B10202), 1–19.

Hirth, G., Tullis, J., 1992. Dislocation creep regimes in quartz aggregates. Journal of Structural Geology 14, 145–159.

Huang, R.Q., Wang, Z., Pei, S.P., Wang, Y.S., 2009. Crustal ductile flow and its contribution to tectonic stress in Southern China. Tectonophysics 473, 476–489.

Ji, J.Q., Zhong, D.L., Sang, H.Q., Qiu, J., Hu, S.L., 2000. Dating of two metamorphic events on the basalt granulite from the Nabang area on the border of China and Burma. Acta Petrologica Sinica 16, 227–232.

Ji, W.Q., Wu, F.Y., Chung, S.L., Li, J.X., Liu, C.Z., 2009. Zircon U–Pb geochronology and Hf isotopic constraints on petrogeneisis of the Gangdese batholith, southern Tibet. Chemical Geology 262, 229–245.

Jolivet, L., Beyssac, O., Goffe, B., Avigad, D., Lepvrier, C., Maluski, H., Thang, T.T., 2001. Oligo-miocene midcrustal subhorizontal shear zone in Indochina. Tectonics 20, 46–57.

Jones, R.R., Holdsworth, R.E., Bailey, W., 1997. Lateral extrusion in transpression zones: the importance of boundary conditions. Journal of Structural Geology 19, 1201–1217.

Jones, R.R., Holdsworth, R.E., Clegg, P., McCaffrey, K., Tavarnelli, E., 2004. Inclined transpression. Journal of Structural Geology 26, 1531–1548.

Langille, J., Lee, J., Hacker, B., Seward, G., 2010. Middle crustal ductile deformation patterns in southern Tibet: insights from vorticity studies in Mabja Dome. Journal of Structural Geology 32, 70–85.
Lee, H.Y., Chung, S.L., Wang, J.R., Wen, D.J., Lo, C.H., Yang, T.F., Zhang, Y.Q., Xie, Y.W., Lee, T.Y., Wu, G.Y., Ji, J.Q., 2003. Miocene Jiali faulting and its implication for Tibetan tectonic evolution. Earth and Planetary Science Letters 205, 185–194.
Lei, Y.L., Ji, J.Q., Gong, D.H., Zhong, D.L., Wang, X.S., Zhang, J., Wang, X.M., 2006. Thermal and denudational history of granitoid batholith recorded by apatite fission track in the Dulong River region in northwestern Yunnan since Late Miocene. Acta Petrologica Sinica 22, 938–948.
Leloup, P.H., Arnaud, N., Lacassin, R., Kienast, J.R., Harrison, T.M., Trong, T.T.P., Replumaz, A., Tapponnier, P., 2001. New constraints on the structure, thermochronology and timing of the Ailao Shan-Red River shear zone, SE Asia. Journal of Geophysical Research 106, 6683–6732.
Leloup, P.H., Lasassin, R., Tapponnier, P., Scharer, U., Dalai, Z., Xiaohan, L., Liangshang, Z., Shaocheng, J., Trinh, P.T., 1995. The Ailao Shan-Red River shear zone (Yunnan, China), Cenozoic transform boundary of Indochina. Tectonophysics 251, 3–84.
Lepvrier, C., Maluski, H., Nguyen, V.V., Roques, D., Axente, V., Rangin, C., 1997. Ar/^{39}Ar Indosinian age of NW-trending dextral shear zones within the Truong Son belt (Vietnam): Cretaceous to Cenozoic overprinting. Tectonophysics 283, 105–127.
Li, Y.H., Wu, Q.J., Zhang, R.Q., Tian, X.B., Zeng, R.S., 2008. The crust and upper mantle structure beneath Yunnan from joint inversion of receiver functions and Rayleigh wave dispersion data. Physics of the Earth and Planetary Interiors 170, 134–146.
Lin, T.H., Lo, C.H., Chung, S.L., Hsu, F.J., Yeh, M.W., Lee, T.Y., Ji, J.Q., Wang, Y.Z., Liu, D.Y., 2009. Ar/^{39}Ar dating of the Jiali and Gaoligong shear zones: implications for crustal deformation around the Eastern Himalayan Syntaxis. Journal of Asian Earth Sciences 34, 674–685.
Lister, G.S., Hobbs, B.E., 1980. The simulation of fabric development during plastic deformation and its application to quartzite: the influence of deformation history. Journal of Structural Geology 2, 335–352.
Lister, G.S., Paterson, M.S., 1979. The simulation of fabric development during plastic deformation and its application to quartzite: fabric transitions. Journal of Structural Geology 1, 99–115.
Mancktelow, N.S., Pennacchioni, G., 2004. The influence of grain boundary fluids on the microstructure of quartz-feldspar mylonites. Journal of Structural Geology 26, 47–69.
Mark, P., Pavlina, H., Christopher, J.L.W., Sandra, P., Karel, S., 2010. Evaluating quartz crystallographic preferred orientations and the role of deformation partitioning using EBSD and fabric analyse techniques. Journal of Structural Geology 32, 803–817.
McDougall, I., Harrison, T.M., 1999. Geochronology and Thermochronology by the ^{40}Ar/^{39}Ar Method. Oxford University Press, New York, pp. 1–269.
Metcalfe, I., 2002. Permian tectonic framework and palaeogeography of SE Asia. Journal of Asian Earth Sciences 20, 551–566.
Morley, C.K., 2007. Variations in Late Cenozoic-Recent strike-slip and oblique-extensional geometries, within Indochina: the influence of pre-existing fabrics. Journal of Structural Geology 29, 36–58.
Passchier, C.W., Trouw, R.A.J., 1996. Microtectonics. Springer Verlag, Berlin, p. 289.
Peternell, M., Hasalová, P., Wilson, J.L., Piazolo, S., Schulmann, K., 2010. Evaluating quartz crystallographic preferred orientations and the role of deformation partitioning using EBSD and fabric analyser techniques. Journal of Structural Geology 32, 803–817.
Ramsay, J.G., Lisle, R.J., 2000. Applications of Continuum Mechanics in structural Geology. In: The Techniques of Modern Structural Geology, vol. 3. Academic Press, London.
Rolland, Y., Cox, S.F., Corsini, M., 2009. Constraining deformation stages in brittle-ductile shear zone from combined field mapping and ^{40}Ar/^{39}Ar dating: the structural evolution of the Grimsel Pass area (Aar Massif, Swiss Alps). Journal of Structural Geology 31, 1377–1394.
Royden, L.H., Burchfiel, B.C., King, R.W., Wang, E., Chen, Z., Shen, F., Yuping, L., 1997. Surface deformation and lower crustal flow in eastern Tibet. Science 276, 788–790.
Searle, M.P., 2006. Role of the Red River shear zone, Yunnan and Vietnam, in the continental extrusion of SE Asia. Journal of the Geological Society 163, 1025–1036. London.
Searle, M.P., Yeh, M.W., Lin, T.-H., Chung, S.L., 2010. Structural constraints on the timing of left-lateral shear along the Red River shear zone in the Ailao Shan and Diancang Shan ranges, Yunnan, SW China. Geosphere 6, 316–338.
Shen, Z.K., Lu, J.N., Wang, M., Rgmann, R.B., 2005. Contemporary crustal deformation around the southeast borderland of the Tibetan Plateau. Journal of Geophysical Research 110 (B11409), 1–17.
Socquet, A., Pubellier, M., 2005. Cenozoic deformation in western Yunnan (China-Myanmar border). Journal of Asian Earth Sciences 24, 495–515.
Song, S.G., Niu, Y.L., Wei, C.J., Ji, J.Q., Su, L., 2010. Metamorphism, anatexis, zircon ages and tectonic evolution of the Gongshan block in the northern Indochina continent – an eastern extension of the Lhasa Block. Lithos 120, 327–346.
Stipp, M., Kunze, K., 2008. Dynamic recrystallization near the brittle-plastic transition in naturally and experimentally deformed quartz aggregates. Tectonophysics 448, 77–97.
Tapponnier, P., Peltzer, G., Armij, R.O., Le Dain, A.Y., Cobbold, P., 1982. Propagating extrusion tectonics in Asia: new insights from simple experiments with plasticine. Geology 10, 611–616.
Tapponnier, P., Xu, Z.Q., Roger, F., Meyer, B., Arnaud, N., Wittlinger, G., Yang, J.S., 2001. Oblique stepwise rise and growth of the Tibet plateau. Science 294, 1671–1677.
Toy, V.G., Prior, D.J., Norris, R.J., 2008. Quartz fabrics in the Alpine Fault mylonites: influence of pre-existing preferred orientations on fabric development during progressive uplift. Journal of Structural Geology 30, 602–621.
Trepmann, C., Lenze, A., Stockhert, B., 2010. Static recrystallization of vein quartz pebbles in a high-pressure-low-temperature metamorphic conglomerate. Journal of Structural Geology 32, 202–215.
Wallis, S.R., Behrmann, J.H., 1996. Crustal stacking and extension recorded by tectonic fabrics of the SE margin of the Tauern Window, Austria. Journal of Structural Geology 18, 1455–1470.
Wang, E.Q., Burchfiel, B.C., 1997. Interpretation of Cenozoic tectonics in the right lateral accommodation zone between the Ailao Shan shear zone and the eastern Himalayan syntaxis. International Geology Review 39, 191–219.
Wang, E.Q., Burchfiel, B.C., Royden, L.H., Chen, L.Z., Chen, J.S., Li, W.X., Chen, Z.L., 1998. Late Cenozoic Xianshuihe–Xiaojiang, Red River, and Dali Fault Systems of Southwestern Sichuan and Central Yunnan, China. Special Paper. In: Geological Society of America, vol. 327, pp. 1–108.
Wang, G., Wan, J.L., Wang, E.Q., Zheng, D.W., Li, F., 2008. Late Cenozoic to recent transtensional deformation across the Southern part of the Gaoligong shear zone between the Indian plate and SE margin of the Tibetan plateau and its tectonic origin. Tectonophysics 460, 1–20.
Wang, Y.J., Fan, W.M., Zhang, Y.H., Peng, T.P., Chen, X.Y., Xu, Y.G., 2006. Kinematics and ^{40}Ar/^{39}Ar geochronology of the Gaoligong and Chongshan shear systems, western Yunnan, China: implications for early Oligocene tectonic extrusion of SE Asia. Tectonophysics 418, 235–254.
Xu, Y.G., Lan, J.B., Yang, Q.J., Huang, X.L., Qiu, H.N., 2008. Eocene break-off of the Neo-Tethyan slab as inferred from intraplate-type mafic dykes in the Gaoligong orogenic belt, eastern Tibet. Chemical Geology 255, 439–453.
Yeh, M.W., Lee, T.Y., Lo, C.H., Chung, S.L., Lan, C.Y., Anh, T.T., 2008. Structural evolution of the day Nui Con Voi metamorphic complex: implications on the development of the Red River shear zone, northern Vietnam. Journal of Structural Geology 30, 1540–1553.
Yin, A., Harrison, T.M., 2000. Geologic evolution of the Himalayan-Tibetan orogen. Annual Review of Earth and Planetary Sciences 28, 211–280.
Zhang, B., Zhang, J.J., Zhong, D.L., 2010. Structure, kinematics and ages of transpression during strain partitioning in the Chongshan shear zone, western Yunnan, China. Journal of Structural Geology 32, 445–463.
Zhang, J.J., Zhong, D.L., Sang, H.Q., Zhou, Y., 2006. Structural and geochronological evidence for multiple episodes of tertiary deformation along the AilaoShan-Red River shear zone, Southeastern Asia, since the Paleocene. Acta Geologica Sinica 80, 79–96.
Zhang, L.S., Schärer, U., 1999. Age and origin of magmatism along the Cenozoic Red-River shear belt, China. Contributions to Mineralogy and Petrology 134, 67–85.
Zhang, X., Wang, Y.H., 2009. Crustal and upper mantle velocity structure in Yunnan, Southern China. Tectonophysics 471, 171–185.
Zhong, D.L., 2000. Paleotethysides in West Yunnan and Sichuan, China. Science Press, Beijing, pp. 37–248.

Further reading

Bestmann, M., Prior, D.J., 2003. Intragranular dynamic recrystallization in naturally deformed calcite marble: diffusion accommodated grain boundary sliding as a result of subgrain rotation recrystallization. Journal of Structural Geology 25, 1597–1613.
Dalrymple, G.B., Lanphere, M.A., 1971. Ar/^{39}Ar technique of K-Ar dating: a comparison with the conventional technique. Earth and Planetary Science Letters 12, 300–308.
Harrison, T.M., Ducan, I., McDougall, I., 1985. Diffusion of ^{40}Ar in biotite: temperature, pressure and compositional effects. Geochimica et Cosmochimica Acta 49, 2461–2468.